THE UNIVERSITY OF CHICAGO

NEURAL CODING AND SENSORY MODULATION IN THE CUNEATE NUCLEUS OF PRIMATES

A DISSERTATION SUBMITTED TO
THE FACULTY OF THE DIVISION OF THE BIOLOGICAL SCIENCES
AND THE PRITZKER SCHOOL OF MEDICINE
IN CANDIDACY FOR THE DEGREE OF
DOCTOR OF PHILOSOPHY

COMMITTEE ON COMPUTATIONAL NEUROSCIENCE

BY
QINPU HE

CHICAGO, ILLINOIS
DECEMBER 2021

Table of Contents

List of Figures

List of Supplementary Figures

Acknowledgments

Advisor
Sliman Bensmaia

Thesis Committee
Murray Sherman
Lee Miller
Matt Kaufman

Neurosurgeon
Joshua Rosenow

Bensmaia Lab

Previous Mentors
KatieAnn Skogsberg
Christine Shannon

Family
My mother Zhengwei Luo
My husband Guangpu Li
My father Chunsheng He
My grandmather Shuzhen Hu and grandfather Zhongzhi Luo

Dedication| To my mother: Thank you for offering everything you could to raise me up

Abstract

The sense of touch is one of our most important channels for communicating with the environment. While vision allows us to identify and locate objects in space, somatosensation is the only sensation that provides direct information about contacting with objects that allows us to interact with them effectively (Delhaye et al., 2018). From picking up a cup to drink, to grasp a pen to write, to touch our loved ones and express our emotions, touch plays an important role in our affective lives and is critical to our ability to dexterously interact with objects (Hertenstein et al., 2006). Indeed, tactile feedback is indispensable to make smooth and precise movement execution, patients who lack tactile signals could not achieve smooth motor execution (Augurelle et al., 2003). However, our understanding of tactile processing differs along various stages of the tactile ascending pathway. In primates, the coding of tactile information has been extensively studied in the nerve and in primary somatosensory cortex (S1) while our understanding of the middle structures, the dorsal column nuclei and the thalamus, are limited. Hence, the goal of my dissertation is to investigate how tactile information is represented at the first synapse along the dorsal-column medial lemniscus pathway (DCML), the Cuneate nucleus (CN), that receives tactile and proprioceptive information from the upper body. I characterized the receptive field structure of CN neurons, determined the convergence of input from multiple sensory channels, documented the temporal and spatial processing of information in CN and investigated the state dependence of cutaneous sensitivity in CN. Overall, I gained understanding of the process and calculations happening at this previously neglected region.

Chapter 1 | Introduction

1.1 Introduction

In primates, the coding of tactile information has been extensively studied in the nerve and in somatosensory cortex (SC). In contrast, the study of the intermediate structures, the dorsal column nuclei and the thalamus, has been far more limited. The main objective of my graduate work has been to investigate how tactile information is represented at the first synapse along the dorsal-column medial lemniscus pathway (DCML), the cuneate nucleus (CN), which receives tactile and proprioceptive signals from the upper body. I characterized the receptive field structure and response properties of CN neurons and showed that cutaneous signals in CN are modulated depending on behavioral state by top down signals.

1.2 Tactile processing pathway

A central question in sensory neuroscience is how sensory information is represented and transformed at different stages along the neuraxis. My work focuses on the dorsal column-medial lemniscus (DCML) pathway of primates, the primary neuraxis for touch and proprioception (Figure 1.1). At the somatosensory periphery, touch arises from the transduction of mechanical deformations of the skin by different types of mechanoreceptors. The first recipients of signals from the somatosensory periphery are the dorsal column nuclei in the medulla, after a brief ascent of the ipsilateral dorsal column. Signals from the upper body project to the cuneate and external cuneate nuclei while signals from the lower body to the gracile nucleus. Projections from these dorsal column nuclei decussate and synapse onto the ventroposterior lateral nucleus of the thalamus, which in turn projects to the somatosensory cortex, with the bulk of them projecting to Brodmann's areas 3b and 1, and a few of them to areas 3a, 2 and 5.

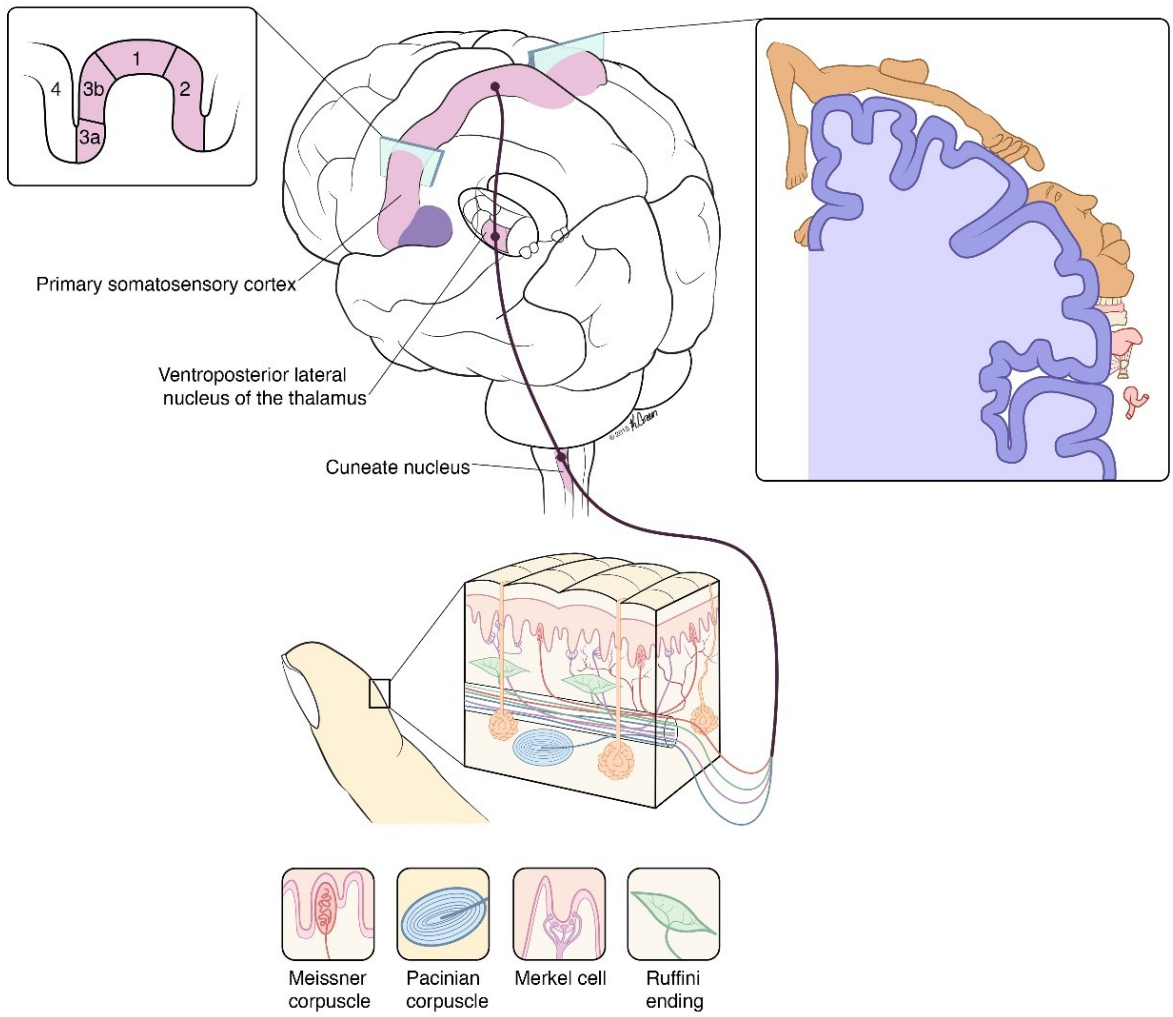

Figure 1.1: Medial lemniscal pathway for the sense of touch (Goodman and Bensmaia, 2018).

1.3 Cutaneous mechanoreceptors and their associated periphery nerves

Our skin contains different types of receptors responding to different stimulus modality. Thermoreceptors respond to non-noxious changes in temperature, nociceptors to strong mechanical, thermal, and chemical stimuli, and low threshold mechanoreceptors to non-noxious skin deformations. A total of four types of mechanoreceptors respond to skin deformations of

the palmar surface of the hand: Merkel cells, Meissner corpuscles, Pacinian corpuscles, and Ruffini endings (Figure 1.1). Ion channels – in particular Piezo2 –in the cell membrane of these mechanoreceptors generate currents in response to mechanical stimulation of the skin and these electrical signals are then carried to the brain by large diameter A nerve fibers (Coste et al., 2010; Woo et al., 2014).

Merkel cells innervate slowly adapting type I afferent (SA1). As their name implies, slowly adapting afferents produce a sustained response to indentations which slowly decreases over tens of seconds or minutes (Figure 1.2) (Knibestöl, 1975). Merkels cells have small receptive field (RF), densely innervate the glabrous skin (80 units per cm^2) and are sensitive to low-frequency skin vibrations (<30 Hz). Given their density and small receptive fields, populations of SA1 nerve fibers convey information about spatial patterns of skin deformations at a high resolution (Phillips et al., 1988a).

Meissner corpuscles are oval in shape and composed of several irregularly-arranged lamellar discs with serrated edges that bend axon terminals of rapidly adapting (RA) afferents during the initial mechanical loading. During the sustained contact, the viscoelastic region at the center of these discs absorbs the stress and lead to RA's phasic response, restricted to the dynamic epochs of an indentation (onset and offset) (Takahashi-Iwanaga and Shimoda, 2003). RA fibers have small RFs, though larger than their SA1 counterparts, and innervate the glabrous skin very densely (140 units per cm^2). RA afferents respond best to skin vibrations at intermediate frequencies (peak around 60 Hz) (Freeman and Johnson, 1982; Muniak et al., 2007).

Pacinian corpuscles are oval in shape and consist of concentric lamellae with layers of viscous fluid between them (Pease and Quilliam, 1957), which shield the afferent in the center from static deformations while allowing high frequency components to pass through. This structure endows PC fibers with rapidly adapting characteristic and high sensitivity to skin vibrations (peaking in sensitivity around 250 Hz). Because Pacinian corpuscles are located

deep in the subcutaneous fat pads, PC fibers have large diffuse receptive fields.

Ruffini endings are spindle-shaped structures innervated by slowly-adapting type 2 afferents (SA2), which respond to skin stretch. They are absent from the glabrous skin of Rhesus Macaques' hands but present though rare in that of humans (Paré et al., 2002). Ruffini endings are also located deep in the dermis so SA2 fibers have large receptive fields. Ruffini endings are most prevalent around nails and, as a result, SA2 afferents are particularly informative about the direction at which forces are applied on the fingertip (Birznieks et al., 2009).

Pacinian corpuscles are oval in shape and consist of concentric lamellae with layers of viscous fluid between them (Pease and Quilliam, 1957), which shield the afferent in the center from static deformations while allowing high frequency components to pass through. This structure endows PC fibers with rapidly adapting characteristic and high sensitivity to skin vibrations (peaking in sensitivity around 250 Hz). Because Pacinian corpuscles are located deep in the subcutaneous fat pads, PC fibers have large diffuse receptive fields.

The different biomechanical and electrochemical properties of the nerve endings confer to the nerve fibers that innervate them different response properties. Interactions with objects typically activate large populations of nerve fibers of all classes, each of which conveys different but overlapping information about an object grasped in the hand, including its shape, texture, motion, etc (Saal et al., 2015). Next, we consider how different object features and their associated sensory continua are encoded in the nerve.

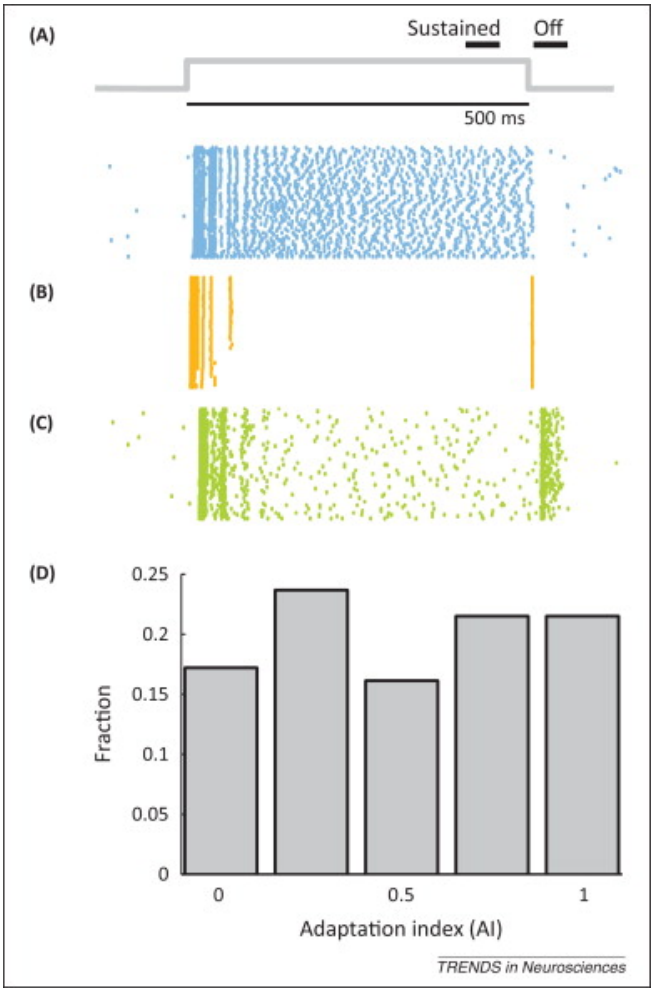

Figure 1.2: Adaptation responses in cortex demonstrate submodality convergence. A| Responses of a typical slowly adapting type 1 (SA1) afferent to 60 repeated presentations of a step indentation lasting 500 ms (depicted by the grey trace at the top). B| Responses of a rapidly adapting (RA) afferent to the same stimulus. C| Response of a typical neuron in area 3b. D| The adaptation index, AI, is determined by the ratio of the OFF response to the SUSTAINED response, each normalized by their respective population means (Saal and Bensmaia, 2014).

1.4 Tactile coding in the periphery nerve

1.4.1 Perceived magnitude

Touch sensations vary over a continuum of intensity, from light to strong, paralleling brightness in vision or loudness in audition. Psychophysical studies have shown that the per-

ceived intensity of a sinusoidal skin vibration grows linearly as a function of its amplitude (Johnson, 1974). The responses of individual nerve fibers to vibrations do not exhibit linear rate-intensity functions. Rather, these functions are piecewise linear, with long plateaus over which changes in amplitude do not result in an increase in the firing rate. Thus, perceived magnitude cannot be explained from the responses of individual nerve fibers. However, when afferent responses are pooled over populations of nerve fibers, the plateaus disappear, and the resulting population firing rate can account for perception if the firing rates are weighted by fiber type. Indeed, SA1 spikes are most strongly weighted, PC spikes are the least weighted, and RA spikes are intermediate (Bensmaia, 2008).

1.4.2 Vibratory frequency

The touch sensations evoked by skin vibrations depend on their frequency, in part because different nerve fibers exhibit different frequency sensitivity profiles: Vibrations below 5 Hz excite primarily SA1 fibers and feel like tapping, vibrations between 5-50 Hz primarily activate RA fibers and feel like flutter, vibrations beyond 50 Hz primarily excite PC fibers and elicit sensations of vibratory hum (Talbot et al., 1968; Ochoa and Torebjörk, 1983). However, sensitivity to changes in frequency is not solely determined by the activated population. Indeed, human observers can reliably detect a 10% change in frequency within the flutter range and a 30% change at the high frequencies (Goff, 1967). Vibratory frequency is encoded in the phase-locked responses of nerve fibers. Indeed, over the range of tangible frequencies, nerve fibers produce one or more spikes within a restricted portion of each stimulus cycle, so the interspike or interburst interval is highly informative about frequency (Talbot et al., 1968). This temporal patterning has been shown to support frequency discrimination (Birznieks and Vickery, 2017) and shapes the percepts evoked by complex skin vibrations (Mackevicius et al., 2012), including those elicited when we scan a textured surface (Weber et al., 2013), to reflect their frequency composition.

1.4.3 Shape

When we grasp an object, cutaneous information signals about local features of the object at each contact point, which is encoded in the responses of tactile nerve fibers, is integrated with information about the conformation of our hand, which is encoded by our proprioceptive nerve fibers, to give rise to a three dimensional percept of the object (Hsiao, 2008), an ability termed stereognosis. The spatial features of object grasped are reflected in the spatial pattern of activation evoked in SA1 and RA afferents (Johnson and Lamb, 1981; Phillips et al., 1988b; Goodwin et al., 1995; Wheat and Goodwin, 2001). SA1 afferents signal the most spatially acute neural image and mediate our ability to discern the smallest tangible feature while RA afferents convey information about coarse spatial features. Meanwhile, our sense of the relative position of different contact points originates from proprioceptors embedded in joints, muscles, tendons, and the skin. How these two sources of information are integrated downstream to give rise to stereognosis is unknown.

1.4.4 Texture

Our sense of touch endows us with an exquisite sensitivity to surface texture. We can discern surface features measured in the tens of nanometers and discriminate features that differ by hundreds of nanometers (Skedung et al., 2013). When we seek to acquire information about surface texture, we scan our fingers across it (Lederman and Klatzky, 1993).Texture perception is mediated by two different neuronal mechanisms: a spatial mechanism mediated by SA1 and RA afferents (Blake et al., 1997) and a temporal one mechanism mediated by RA and PC afferents (Lamb, 1983; Weber et al., 2013). Indeed, the spatial layout of coarse textural features is encoded in a neural image carried by populations of the SA1 and RA fibers (Blake et al., 1997). To discern fine textural features requires movement between skin and surface, which leads to the elicitation of texture-specific vibrations that spread over wide swaths of skin (Hollins and Risner, 2000). These vibrations give rise to texture specific

temporal spiking patterns in PC and RA fibers that carry information about texture identity with a temporal precision that is measured in single-digit milliseconds (Weber et al., 2013). Our ability to sense textural features that span six orders of magnitude in spatial scale (from tens of nanometers to tens of millimeters) is made possible by the integration of these two neural codes for texture, spatial and temporal.

1.4.5 Motion

Manual interactions with objects typically involve motion between the hand and the object and when we explore objects to sense their shape or texture, we move our hands across them (Lederman and Klatzky, 1993). Accordingly, information about the direction and speed of motion is available via the sense of touch. Two mechanisms mediate our ability to sense the direction of motion. First, movement across the skin sequentially activates nerve fibers with receptive fields along the path of motion (Pei and Bensmaia, 2014), as is observed for motion signals on the retina (Pack and Bensmaia, 2015). Second, lateral movement between object and hand stretches the skin and activates sensitive SA2 fibers, which in turn can signal direction of motion (Olausson et al., 2000). While we can perceive the speed at which objects move across the skin, which is mainly mediated by PC fibers, our ability to do so is highly dependent on the texture of the surface (Dépeault et al., 2008; Delhaye et al., 2019).

1.5 Tactile coding in the brain stem nuclei

Tactile nerve fibers innervating the hand project onto neurons in the cuneate nucleus (CN). The CN (along with the gracile nucleus, which receives input from the lower body) has been traditionally viewed as passive relay stations that faithfully transmit afferent input to the thalamus (Vickery et al., 1994; Gynther et al., 1995). However, CN responses have never been systematically compared to their afferent inputs, which precludes any conclusions as to its contribution to sensory processing. In Chapter two, I discuss our work demonstrating

that the responses of individual CN neurons reflect the integration of inputs from multiple classes of nerve fibers and that these inputs are subject to neuronal computations, such that CN responses are more similar to cortical responses than they are to peripheral ones. In Chapter three, I discuss our work showing that cutaneous responses in CN are modulated according to the behavioral state of the animal, further challenging the idea that CN is just a passive relay station for somatosensory signals.

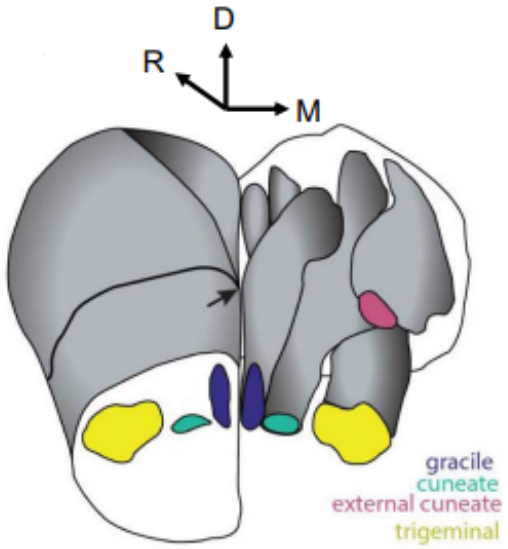

Figure 1.3: Positioning of brain stem nuclei. A reconstructed 3D view of the lower brain stem and relative positioning of the gracile nucleus, cuneate nucleus, external cuneate nucleus, and trigeminal nucleus. Black arrow is pointing toward obex (Suresh et al., 2017).

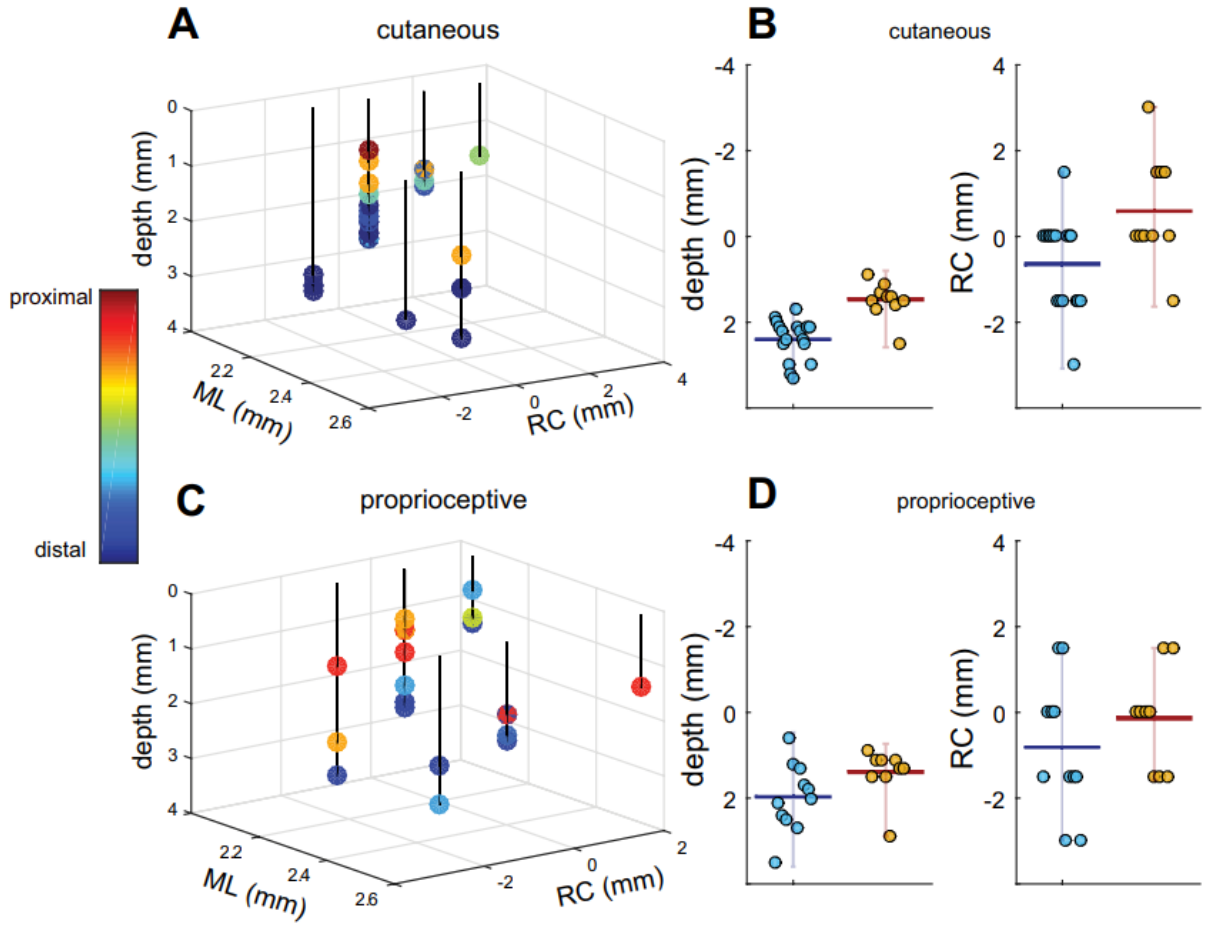

Figure 1.4: Somatotopic organization of CN. A| 3D diagram of penetrations with cutaneous RFs plotted with respect to obex and the surface. Color bar indicates the RF location. ML, medio-lateral; RC, rostro-caudal. B| Summary of cutaneous results. Left: distal units tend to be deeper than proximal units. Horizontal bar represents mean values, and vertical bars span the range of values. Right: distal units tend be more cranial (negative along the RC dimension) than proximal units. The forearm served as the boundary between distal and proximal units in the bar plots. C| 3D diagram of penetrations with proprioceptive responses with respect to obex and the surface. Color bar indicates RF location. D| Summary of proprioceptive results. Left: distal units tend to be deeper than proximal units. Right: distal units tend to be anterior to their proximal counterparts. Overall, both proprioceptive and cutaneous modalities exhibited similar somatotopic trends: proximal units were located more superficially and more posterior to the obex than distal units. Reproduced from (Suresh et al., 2017).

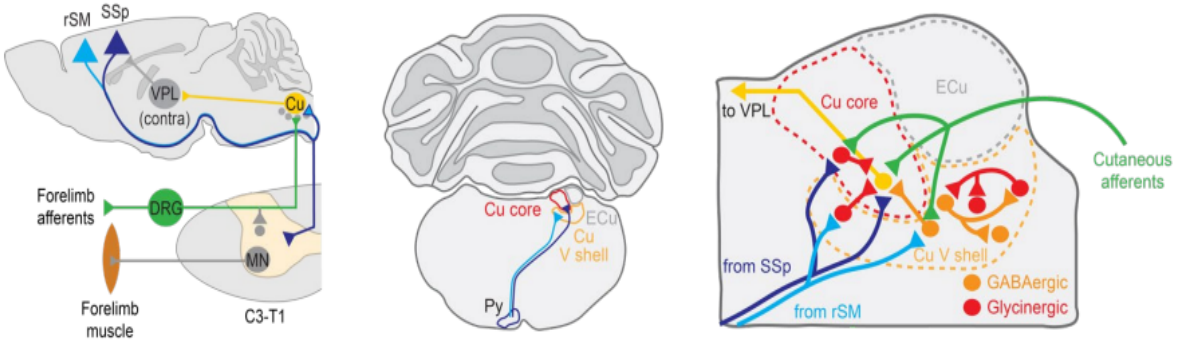

Figure 1.5: Distinct corticofugal pathways target cuneate circuits. The main cuneate nucleus is a major conduit of forelimb sensory information to supraspinal regions, including the neocortex, via cuneolemniscal projections (yellow) to the thalamus (VPL). The core region of the middle CN receives direct input from cutaneous afferents (green) that innervate the glabrous pad of the hand and reside in the dorsal root ganglia (DRG). GABAergic neurons (orange) located largely in the cuneate ventral shell (V shell) and glycinergic neurons (red) located in the cuneate ventral shell and cuneate core directly inhibit cuneolemniscal neurons. These inhibitory neurons receive inhibitory input, potentially from local connections, and also receive direct input from ascending cutaneous afferents. The cuneate core region is heavily targeted by corticospinal neurons residing in primary somatosensory cortex (SSp; dark blue), and cuneolemniscal neurons that reside in this core region receive direct input from SSp projections. Inhibitory cuneate neurons also receive SSp input, but unlike cuneolemniscal neurons, are also targeted by corticofugal neurons in rostral sensorimotor cortex (rSM; light blue), which do not project to the cuneate core, but rather target the shell region ventral to the cuneate. Cuneate inhibitory circuits provide a means for bidirectional modulation of the transmission of tactile information through the cuneate core, and their activation or inhibition perturbs the execution of tactile guided dexterous behaviors. ECu, external cuneate; Py, pyramidal tract. (Conner et al., 2021).

1.5.1 Brainstem nuclei

Four dorsal column nuclei (DCN) in the brainstem are implicated in somatosensory processing (Loutit et al., 2020). The CN, which receives both tactile and proprioceptive input from the upper body, external cuneate nucleus (ECN), which receives proprioceptive information from the upper body, the gracile nucleus (GN), which receives tactile and proprioceptive input from the lower body, and the trigeminal nucleus (TN), which receives tactile and proprioceptive input from the face. The GN is located most medially, spanning the first 1.25 to

1.5 mm lateral to midline. Next are the CN and ECN, which span 1.5 to 1.75 mm (Suresh et al., 2017). The TN then spans another millimeter or so along the medio-lateral axis (Figure 1.3, Figure 1.4). While the boundary between CN and ECN is distinct anatomically, it is hard to distinguish electrophysiologically.

Functional organization of the CN

In rhesus macaques, both CN and ECN exhibit a coarse somatotopic organization along both the rostro-caudal and dorsal-ventral axis, with units innervating the distal limbs tending to be located deeper and more rostral than units innervating the proximal limb (Suresh et al., 2017). A similar dorsal-ventral somatotopic trend has been reported in other primate species while the rostral-caudal trends seem to be specific to macaques (Florence et al., 1989; Qi and Kaas, 2006). The representation of the digits tends to be located more ventromedially than that of the rest of the hand in rhesus macaques while other species of non-human primates exhibit the reverse trend (Florence et al., 1989). The digit representation in macaques is especially difficult to access given its location under the cerebellar tonsils. The representation of the trunk lies in the transition zone between CN and its medial neighbor GN while the representation of the head lies on the lateral aspect of the CN, neighboring face representations in TN (Millar and Basbaum, 1975; Li et al., 2012).

Cutaneous and proprioceptive information remain segregated at the level of dorsal column nuclei. Proprioceptive units tend to be more superficial and more lateral than cutaneous ones and more frequently caudal to the obex in rhesus macaques (Suresh et al., 2017). While CN receives both proprioceptive and cutaneous input, the ECN receives exclusively proprioceptive input.

Targets of CN

The DCN act as a distribution hub for tactile and proprioceptive signals, projecting to a wide variety of targets throughout the spinal cord and brain. CN sends its major projection to the contralateral ventro-posterior lateral nuclei of the thalamus (VPL) via the medial lemniscus. VPL then projects to somatosensory cortex, located in the anterior aspect of the parietal lobe, including Brodmann's areas 3a, 3b, 1, and 2.

In contrast, ECN projects primarily to the cerebellum, and this cuneocerebellar pathway is the primary source of cerebellar inputs from upper-body proprioceptors (Paxinos et al., 2012). Proprioceptive signals from the dorsal column nuclei also project onto the border of VPL and ventrolateral nucleus (VL) of the thalamus (Berkley et al., 1986), which then mainly target area 3a, as well as areas 2 and 3b (Padberg et al., 2009).

Besides VPL and cerebellum, CN and ECN also project to other spinal and supraspinal recipients in rodents and cats, including the contralateral posterior group of the thalamus (Diamond et al., 1992), the nucleus reuniens (Villanueva et al., 1998), the Pontine nuclei (Kosinski et al., 1988), the superior colliculus (Blomqvist et al., 1978; Nagata and Kruger, 1979), and the inferior colliculus (Aitkin et al., 1981; Wiberg et al., 1987).

Descending inputs into CN

CN also receives significant projections from cortex, which have recently been characterized in detail in mice (Conner et al., 2021). The mouse CN can be divided into two regions: a core region that receives the bulk of the input from the periphery and an outer shell that comprises mostly inhibitory interneurons (Conner et al., 2021). Each region receives a distinct pattern of projections from cortex: The core region receives excitatory inputs from somatosensory cortex whereas the shell receives both excitatory and inhibitory input from a variety of motor structures. The CN of primates has also been shown to receive both excitatory and inhibitory projections from cortex and these descending inputs match both

the modality and the response field of their targets. That is, M1 and area 3a mainly project onto proprioceptive areas in the DCN while (cutaneous) area 3b projections to touch-related CN regions (Cheema et al., 1983; Cheema et al., 1985; Kuypers et al., 1961). In addition, the response fields of the central neurons and their CN targets match (Cheema et al., 1985).

Convergence of cutaneous submodalities in CN

Traditionally, the different tactile submodalities – each associated with a different cutaneous mechanoreceptor and its associated neurite – were thought to remain segregated as they ascend the neuraxis. In this view, signals from each type of nerve fibers projected onto different largely non-overlapping populations of neurons and these different channels of tactile information were hypothesized to play different functional roles in tactile perception. However, quantitative examination of responses in primary somatosensory cortex (Brodmann's area 3b) reveals that, even at the earliest stage of cortical processing, the responses of individual neurons reflect input from multiple classes of tactile nerve fibers (Pei et al., 2009; Saal et al., 2015b). Furthermore, the perception of several tactile features – the perceived magnitude of a vibration or the roughness of a texture – has been shown to reflect convergent input from multiple modalities, calling into question the functional segregation hypothesized by the traditional view (Muniak et al., 2007a; Weber et al., 2013; Lieber et al., 2017).

In chapter two, I will discuss our recent work showing that the convergence of different submodality signals onto individual neurons is already observed in the CN (Suresh et al., 2021). Indeed, individual CN neurons exhibit response properties indicative of convergent input from both slowly adapting and rapidly adapting nerve fibers. In addition, many CN neurons respond to a wide range of vibratory frequencies, exhibiting a much wider bandwidth than any one population of nerve fibers.

1.5.2 Tactile coding in somatosensory cortex

CN neurons mainly project to the VPL of the thalamus, which then projects to the somatosensory cortex (SC), including Brodmann's areas 3a, 3b, 1 and 2. SC is organized somatotopically such that nearby neurons have nearby receptive fields (Pons et al., 1985). The hand representation in SC is highly enlarged, reflecting its outsized role in object interactions (Sur et al., 1980). While cutaneous nerve fibers reflect the local skin deformation in highly predictable ways that depend only on their class, SC neurons exhibit more complex and diverse response properties, giving rise to a high dimensional representation of their inputs. For example, individual SC neurons exhibit a selectivity for stimulus features such as orientation and motion direction. These response properties of cortical neurons have heretofore been thought to first emerge in SC. One of the objectives of the study described in Chapter 2 was to assess the degree to which the elaborated response properties of SC neurons might reflect computations inherited from their inputs. To this end, we measured CN responses to two classes of stimuli that have been extensively used to characterized afferent and SC response, namely vibrations (Mountcastle et al., 1969; Harvey et al., 2013; Saal et al., 2015b) and oriented edges (Bensmaia et al., 2008; Pruszynski and Johansson, 2014).

Temporal response properties

As discussed above, the different classes of nerve fibers differ in their frequency sensitivity profiles such that SA1 fibers peak in sensitivity at low frequencies (<10 Hz), PC fibers at high frequencies ($\sim 250Hz$, and RA fibers at intermediate frequencies (Talbot et al., 1968b; Muniak et al., 2007). SC neurons exhibit a wide range of frequency sensitivity profiles. Importantly, individual SC neurons often respond over a wider range of frequencies than any one population of nerve fibers, implying that they receive convergent inputs from multiple classes of afferents. Furthermore, vibratory responses of SC neuron often reflect temporal computations on their inputs (Saal et al., 2015). Indeed, while some SC neurons integrate

afferent signals over time, others act as more complex temporal filters, often consisting of an excitatory and inhibitory lobe. These neurons act as temporal differentiators and respond to specific features in the input. Furthermore, the shape of these filters differ systematically depending on the input modality: The filters for SA1 and RA inputs comprise large excitatory lobes such that signals from these afferent classes tend to modulate the strength of SC responses to skin vibrations. In contrast, filters for PC inputs comprise balanced or inhibitory lobes and tend to shape the timing rather than the strength of SC responses (Saal et al., 2015). The idiosyncratic shape the temporal filter that describes each neurons vibratory response confers to that neuron a preference for a temporal feature in its time-varying inputs. In summary, then, SC neurons differ in the submodality composition of their inputs and in how they integrate these inputs.

Spatial response properties

While the RFs of SA1 and RA nerve fibers typically comprise one or more small excitatory lobes restricted to a small patch of skin, the diameter of which is measured in single millimeters (Vega-Bermudez and Johnson, 1999; Pruszynski and Johansson, 2014), the RFs of PC fibers are much larger and more diffuse, often spanning multiple digits and sometimes the entire hand. However, all three nerve fibers exhibit responses that track local skin deformation (Kim, S.S. et al., 2010; Saal et al., 2017). In contrast, the RFs of neurons in Brodmann's area 3b are often comprised of both excitatory and inhibitory subfields (DiCarlo and Johnson, 2000) as well as a co-localized but delayed inhibitory component, which makes them less excitable for certain time after excitation (Gardner and Costanzo, 1980; DiCarlo and Johnson, 2000). The structure of the cortical neurons confers to them selectivity for spatial features, for example the orientation of an edge indented into or scanned across the skin. Indeed, more than 50% of SC neurons are orientation tuned (Bensmaia et al., 2008). This orientation tuning has tacitly been assumed to arise de novo in SC.

1.6 References

Aitkin LM, Kenyon CE, Philpott P (1981) The representation of the auditory and somatosensory systems in the external nucleus of the cat inferior colliculus. Journal of Comparative Neurology 196:25–40.

Bensmaia SJ (2008) Tactile intensity and population codes. Behav Brain Res 190:165–173.

Bensmaia SJ, Denchev PV, Dammann JF, Craig JC, Hsiao SS (2008) The Representation of Stimulus Orientation in the Early Stages of Somatosensory Processing. Journal of Neuroscience 28:776–786.

Berkley KJ, Budell RJ, Blomqvist A, Bull M (1986) Output systems of the dorsal column nuclei in the cat. Brain Research Reviews 11:199–225.

Birznieks I, Macefield VG, Westling G, Johansson RS (2009) Slowly Adapting Mechanoreceptors in the Borders of the Human Fingernail Encode Fingertip Forces. Journal of Neuroscience 29:9370–9379.

Birznieks I, Vickery R (2017) Spike Timing Matters in Novel Neuronal Code Involved in Vibrotactile Frequency Perception: Current Biology. Current Biology 27:1485–1490.

Blake DT, Hsiao SS, Johnson KO (1997) Neural Coding Mechanisms in Tactile Pattern Recognition: The Relative Contributions of Slowly and Rapidly Adapting Mechanoreceptors to Perceived Roughness. J Neurosci 17:7480–7489.

Blomqvist A, Flink R, Bowsher D, Griph S, Westman J (1978) Tectal and thalamic projections of dorsal column and lateral cervical nuclei: a quantitative study in the cat. Brain Research 141:335–341.

Bologna LL, Pinoteau J, Brasselet R, Maggiali M, Arleo A (2011) Encoding/decoding of first and second order tactile afferents in a neurorobotic application. Journal of Physiology-Paris:S0928425711000234.

Cheema S, Rustioni A, Whitsel BL (1985) Sensorimotor cortical projections to the primate cuneate nucleus. Journal of Comparative Neurology 240:196–211.

Conner JM, Bohannon A, Igarashi M, Taniguchi J, Baltar N, Azim E (2021) Modulation of tactile feedback for the execution of dexterous movement. Neuroscience.

Coste B, Mathur J, Schmidt M, Earley TJ, Ranade S, Petrus MJ, Dubin AE, Patapoutian A (2010) Piezo1 and Piezo2 are essential components of distinct mechanically-activated cation channels. Science 330:55–60.

Delhaye, B. P., O'Donnell, M. K., Lieber, J. D., McLellan, K. R., Bensmaia, S. J. (2019). Feeling fooled: Texture contaminates the neural code for tactile speed. PLoS biology, 17(8), e3000431.

Dépeault A, Meftah E-M, Chapman CE (2008) Tactile Speed Scaling: Contributions of Time and Space. Journal of Neurophysiology 99:1422–1434.

Diamond ME, Armstrong-James M, Ebner FF (1992) Somatic sensory responses in the rostral sector of the posterior group (POm) and in the ventral posterior medial nucleus (VPM) of the rat thalamus. Journal of Comparative Neurology 318:462–476.

DiCarlo JJ, Johnson KO (2000) Spatial and Temporal Structure of Receptive Fields in Primate Somatosensory Area 3b: Effects of Stimulus Scanning Direction and Orientation. J Neurosci 20:495–510.

Fitzgerald PJ, Lane JW, Thakur PH, Hsiao SS (2006) Receptive Field Properties of the Macaque Second Somatosensory Cortex: Representation of Orientation on Different Finger Pads. Journal of Neuroscience 26:6473–6484.

Florence SL, Wall JT, Kaas JH (1989) Somatotopic organization of inputs from the hand to the spinal gray and cuneate nucleus of monkeys with observations on the cuneate nucleus of humans. Journal of Comparative Neurology 286:48–70.

Freeman AW, Johnson KO (1982) Cutaneous mechanoreceptors in macaque monkey: temporal discharge patterns evoked by vibration, and a receptor model. The Journal of Physiology 323:21–41.

Gardner EP, Costanzo RM (1980) Temporal integration of multiple-point stimuli in pri-

mary somatosensory cortical receptive fields of alert monkeys. Journal of Neurophysiology 43:444–468.

Goff GD (1967) Differential discrimination of frequency of cutaneous mechanical vibration. Journal of Experimental Psychology 74:294–299.

Goodwin A, Browning A, Wheat H (1995) Representation of curved surfaces in responses of mechanoreceptive afferent fibers innervating the monkey's fingerpad. J Neurosci 15:798–810.

Gynther, B. D., Vickery, R. M., Rowe, M. J. (1995). Transmission characteristics for the 1: 1 linkage between slowly adapting type II fibers and their cuneate target neurons in cat. Experimental brain research, 105(1), 67-75.

Harvey MA, Saal HP, Dammann JF, Bensmaia SJ (2013) Multiplexing Stimulus Information through Rate and Temporal Codes in Primate Somatosensory Cortex Pack CC, ed. PLoS Biol 11:e1001558.

Hollins M, Risner SR (2000) Evidence for the duplex theory of tactile texture perception. Perception Psychophysics 62:695–705.

Hsiao S (2008) Central mechanisms of tactile shape perception. Current Opinion in Neurobiology 18:418–424.

Iwamura, Y., Tanaka, M., Sakamoto, M., Hikosaka, O. (1983). Converging patterns of finger representation and complex response properties of neurons in area 1 of the first somatosensory cortex of the conscious monkey. Experimental Brain Research, 51(3), 327-337.

Iwamura, Y., Tanaka, M., Sakamoto, M., Hikosaka, O. (1985). Diversity in receptive field properties of vertical neuronal arrays in the crown of the postcentral gyrus of the conscious monkey. Experimental brain research, 58(2), 400-411.

Johnson KO (1974) Reconstruction of population response to a vibratory stimulus in quickly adapting mechanoreceptive afferent fiber population innervating glabrous skin of the monkey. Journal of Neurophysiology 37:48–72.

Johnson KO, Lamb GD (1981) Neural mechanisms of spatial tactile discrimination: neu-

ral patterns evoked by braille-like dot patterns in the monkey. The Journal of Physiology 310:117–144.

Kim, S.S., Sripati, A.P., Bensmaia, S.J. (2010) Predicting the Timing of Spikes Evoked by Tactile Stimulation of the Hand. Journal of Neurophysiology 104:1484–1496.

Knibestöl M (1975) Stimulus-response functions of slowly adapting mechanoreceptors in the human glabrous skin area. The Journal of Physiology 245:63–80.

Kosinski RJ, Lee HS, Mihailoff GA (1988) A double retrograde fluorescent tracing analysis of dorsal column nuclear projections to the basilar pontine nuclei, thalamus, and superior colliculus in the rat. Neuroscience Letters 85:40–46.

Lamb GD (1983) Tactile discrimination of textured surfaces: peripheral neural coding in the monkey. The Journal of Physiology 338:567–587.

Lederman S, Klatzky R (1993) Extracting objects' properties by haptic exploration. Acta psychologica 84:29–40.

Li CX, Yang Q, Waters RS (2012) Functional and structural organization of the forelimb representation in cuneate nucleus in rat. Brain Research 1468:11–28.

Lieber JD, Xia X, Weber AI, Bensmaia SJ (2017) The neural code for tactile roughness in the somatosensory nerves. Journal of Neurophysiology 118:3107–3117.

Loutit, A. J., Vickery, R. M., Potas, J. R. (2021). Functional organization and connectivity of the dorsal column nuclei complex reveals a sensorimotor integration and distribution hub. Journal of Comparative Neurology, 529(1), 187-220.

Mackevicius EL, Best MD, Saal HP, Bensmaia SJ (2012) Millisecond Precision Spike Timing Shapes Tactile Perception. J Neurosci 32:15309–15317.

Millar J, Basbaum AI (1975) Topography of the projection of the body surface of the cat to cuneate and gracile nuclei. Experimental Neurology 49:281–290.

Mountcastle VB, Talbot WH, Sakata H, Hyvärinen J (1969) Cortical neuronal mechanisms in flutter-vibration studied in unanesthetized monkeys. Neuronal periodicity and frequency

discrimination. Journal of Neurophysiology 32:452–484.

Muniak MA, Ray S, Hsiao SS, Dammann JF, Bensmaia SJ (2007a) The Neural Coding of Stimulus Intensity: Linking the Population Response of Mechanoreceptive Afferents with Psychophysical Behavior. Journal of Neuroscience 27:11687–11699.

Muniak MA, Ray S, Hsiao SS, Dammann JF, Bensmaia SJ (2007b) The Neural Coding of Stimulus Intensity: Linking the Population Response of Mechanoreceptive Afferents with Psychophysical Behavior. J Neurosci 27:11687–11699.

Nagata T, Kruger L (1979) Tactile neurons of the superior colliculus of the cat: Input and physiological properties. Brain Research 174:19–37.

Ochoa J, Torebjörk E (1983) Sensations evoked by intraneural microstimulation of single mechanoreceptor units innervating the human hand. The Journal of Physiology 342:633–654.

Olausson H, Wessberg J, Kakuda N (2000) Tactile directional sensibility: peripheral neural mechanisms in man. Brain Research 866:178–187.

Pack CC, Bensmaia SJ (2015) Seeing and Feeling Motion: Canonical Computations in Vision and Touch. PLOS Biology 13:e1002271.

Padberg J, Cerkevich C, Engle J, Rajan AT, Recanzone G, Kaas J, Krubitzer L (2009) Thalamocortical Connections of Parietal Somatosensory Cortical Fields in Macaque Monkeys are Highly Divergent and Convergent. Cerebral Cortex 19:2038–2064.

Paré M, Smith AM, Rice FL (2002) Distribution and terminal arborizations of cutaneous mechanoreceptors in the glabrous finger pads of the monkey. Journal of Comparative Neurology 445:347–359.

Paxinos, G., Huang, X. F., Sengul, G., Watson, C. (2012). Organization of brainstem nuclei.

Pei Y-C, Bensmaia SJ (2014) The neural basis of tactile motion perception. Journal of Neurophysiology 112:3023–3032.

Pei Y-C, Denchev PV, Hsiao SS, Craig JC, Bensmaia SJ (2009) Convergence of Submodality-Specific Input Onto Neurons in Primary Somatosensory Cortex. Journal of Neurophysiology

102:1843–1853.

Phillips JR, Johnson KO, Hsiao SS (1988a) Spatial pattern representation and transformation in monkey somatosensory cortex. PNAS 85:1317–1321.

Phillips JR, Johnson KO, Hsiao SS (1988b) Spatial pattern representation and transformation in monkey somatosensory cortex. Proceedings of the National Academy of Sciences 85:1317–1321.

Pons TP, Garraghty PE, Cusick CG, Kaas JH (1985) The somatotopic organization of area 2 in macaque monkeys. Journal of Comparative Neurology 241:445–466.

Pruszynski JA, Johansson RS (2014) Edge-orientation processing in first-order tactile neurons. Nature Neuroscience 17:1404–1409.

Qi H-X, Kaas JH (2006) Organization of primary afferent projections to the gracile nucleus of the dorsal column system of primates. J Comp Neurol 499:183–217.

Richardson AG, Weigand PK, Sritharan SY, Lucas TH (2016) A chronic neural interface to the macaque dorsal column nuclei. Journal of Neurophysiology 115:2255–2264.

Saal HP, Delhaye BP, Rayhaun BC, Bensmaia SJ (2017) Simulating tactile signals from the whole hand with millisecond precision. Proc Natl Acad Sci USA 114:E5693–E5702.

Saal HP, Harvey MA, Bensmaia SJ (2015a) Rate and timing of cortical responses driven by separate sensory channels. eLife 4:e10450.

Saal HP, Harvey MA, Bensmaia SJ (2015b) Rate and timing of cortical responses driven by separate sensory channels King AJ, ed. eLife 4:e10450.

Skedung L, Arvidsson M, Chung JY, Stafford CM, Berglund B, Rutland MW (2013) Feeling Small: Exploring the Tactile Perception Limits. Sci Rep 3:2617.

Sur M, Merzenich MM, Kaas JH (1980) Magnification, receptive-field area, and "hypercolumn" size in areas 3b and 1 of somatosensory cortex in owl monkeys. Journal of Neurophysiology 44:295–311.

Suresh AK, Winberry JE, Versteeg C, Chowdhury R, Tomlinson T, Rosenow JM, Miller LE,

Bensmaia SJ (2017) Methodological considerations for a chronic neural interface with the cuneate nucleus of macaques. Journal of Neurophysiology 118:3271–3281.

Takahashi-Iwanaga H, Shimoda H (2003) The three-dimensional microanatomy of Meissner corpuscles in monkey palmar skin. J Neurocytol 32:363–371.

Talbot WH, Darian-Smith I, Kornhuber HH, Mountcastle VB (1968a) The sense of flutter-vibration: comparison of the human capacity with response patterns of mechanoreceptive afferents from the monkey hand. Journal of Neurophysiology 31:301–334.

Talbot WH, Darian-Smith I, Kornhuber HH, Mountcastle VB (1968b) The sense of flutter-vibration: comparison of the human capacity with response patterns of mechanoreceptive afferents from the monkey hand. Journal of Neurophysiology 31:301–334.

Vega-Bermudez F, Johnson KO (1999) SA1 and RA Receptive Fields, Response Variability, and Population Responses Mapped with a Probe Array. Journal of Neurophysiology 81:2701–2710.

Vickery RM, Gynther BD, Rowe MJ (1994) Synaptic transmission between single slowly adapting type I fibres and their cuneate target neurones in cat. The Journal of Physiology 474:379–392.

Villanueva L, Desbois C, le Bars D, Bernard J-F (1998) Organization of diencephalic projections from the medullary subnucleus reticularis dorsalis and the adjacent cuneate nucleus: A retrograde and anterograde tracer study in the rat. Journal of Comparative Neurology 390:133–160.

Weber AI, Saal HP, Lieber JD, Cheng J-W, Manfredi LR, Dammann JF, Bensmaia SJ (2013) Spatial and temporal codes mediate the tactile perception of natural textures. Proc Natl Acad Sci USA 110:17107–17112.

Wheat HE, Goodwin AW (2001) Tactile Discrimination of Edge Shape: Limits on Spatial Resolution Imposed by Parameters of the Peripheral Neural Population. J Neurosci 21:7751–7763.

Wiberg M, Westman J, Blomqvist A (1987) Somatosensory projection to the mesencephalon: An anatomical study in the monkey. Journal of Comparative Neurology 264:92–117.

Woo S-H, Ranade S, Weyer AD, Dubin AE, Baba Y, Qiu Z, Petrus M, Miyamoto T, Reddy K, Lumpkin EA, Stucky CL, Patapoutian A (2014) Piezo2 is required for Merkel-cell mechanotransduction. Nature 509:622–626.

Yau JM, Connor CE, Hsiao SS (2013) Representation of tactile curvature in macaque somatosensory area 2. Journal of Neurophysiology 109:2999–3012.

Chapter 2 | Sensory computations in the cuneate nucleus of macaques

2.1 Abstract

Tactile nerve fibers fall into a few classes that can be readily distinguished based on their spatiotemporal response properties. Because nerve fibers reflect local skin deformations, they individually carry ambiguous signals about object features. In contrast, cortical neurons exhibit heterogeneous response properties that reflect computations applied to convergent input from multiple classes of afferents, which confer to them a selectivity for behaviorally relevant features of objects. The conventional view is that these complex response properties arise within the cortex itself, implying that sensory signals are not processed to any significant extent in the two intervening structures – the cuneate nucleus (CN) and the thalamus. To test this hypothesis, we recorded the responses evoked in CN to a battery of stimuli that have been extensively used to characterize tactile coding in both the periphery and cortex, including skin indentations, vibrations, random dot patterns, and scanned edges. We found that CN responses are more similar to their cortical counterparts than they are to their inputs: CN neurons receive input from multiple classes of nerve fibers, they have spatially complex receptive fields, and they exhibit selectivity for object features. Contrary to consensus, then, CN plays a key role in processing tactile information.

2.2 Significance

Perception is the outcome of the sequential processing of sensory signals at multiple stages along the neuraxis. The conventional view is that tactile signals are processed predominantly in the cerebral cortex. We tested this view by investigating the response properties of neurons

1. This manuscript is under review: Suresh, A. K., Greenspon, C. M., He, Q., Rosenow, J. M., Miller, L. E., & Bensmaia, S. J. (2021). Sensory computations in the cuneate nucleus of macaques. bioRxiv.

in the cuneate nucleus (CN), the first potential stage of processing along the primary touch neuraxis. We found that CN responses more nearly resemble those of cortical neurons than they do those of nerve fibers: CN neurons have spatially complex receptive fields reflecting convergent input from multiple classes of nerve fibers and exhibit a selectivity for object features, absent in the nerve. We conclude that CN plays a key, early role in the processing of tactile information.

2.3 Introduction

The coding of tactile information has been extensively studied in the peripheral nerves and in the primary somatosensory cortex (S1, Broadmann's area 3b) of non-human primates, leading to the conclusion that sensory representations in S1 differ from those at the periphery in at least two important ways. First, while cutaneous nerve fibers can be divided into a small number of classes, each responding to a different aspect of skin deformation, individual S1 neurons integrate sensory signals from multiple classes of nerve fibers (Friedman et al., 2004; Kaas, 1983; Lieber and Bensmaia, 2019; Mountcastle, 1957; Paul et al., 1972; Pei et al., 2009; Saal and Bensmaia, 2014). Indeed, while each class of nerve fibers exhibits stereotyped responses to certain stimulus classes, for example skin indentations or sinusoidal vibrations, cortical responses to these same stimuli include features of the responses from multiple tactile classes, or sub-modalities. Second, the responses of cortical neurons reflect computations on these inputs. For example, the spatial receptive fields of S1 neurons comprise excitatory and inhibitory subfields, implying a spatial computation (Bensmaia et al., 2008; DiCarlo et al., 1998). Similarly, S1 neurons act as temporal filters, as evidenced by the fact that their responses to vibrations reflect both integration and differentiation of their inputs in time (Saal et al., 2015). These computations give rise to increasingly explicit rate-based representations of object features, such as the orientation of an edge indented into the skin or the texture of a surface scanned across the skin (Bensmaia et al., 2008; Lieber and Bensmaia,

2019). In contrast to the well-studied peripheral and cortical representations of touch, very little is known about the contribution of the cuneate nucleus (CN) to the processing of tactile information. The textbook view is that CN acts as a simple relay station despite the fact that the response properties of neurons in CN or equivalent brain structures (nucleus principalis, e.g.) exhibit responses that are not identical to those of nerve fibers (Bystrzycka et al., 1977; Ebert et al., 2021; Jörntell et al., 2014; Kaloti et al., 2016; Witham and Baker, 2011), implying some processing. However, CN responses have not been investigated using stimuli whose representation in the nerve and cortex has been quantitatively characterized (Conner et al., 2021; Ebert et al., 2021; Jörntell et al., 2014; Lehnert et al., 2021). This precludes a quantitative analysis of how tactile signals are transformed in this structure. Furthermore, though a significant body of literature exists where the dorsal column nuclei have been lesioned (Halder et al., 2018; Liao et al., 2015, 2018; Qi et al., 2013) that demonstrates that CN is a key part of the medial leminiscal pathway, this approach is limited in that it invariably alters the inputs to all downstream structures, and therefor the specific role of CN cannot be inferred. To fill this gap, we recorded the responses evoked in individual CN neurons to a battery of tactile stimuli that have been extensively used to characterize the response properties of tactile nerve fibers and of neurons in S1, including skin indentations, vibrations, embossed dot patterns, and scanned edges. We then compared CN responses to their upstream (nerve fibers) and downstream counterparts (area 3b or S1, the first stage of processing in cortex (Delhaye et al., 2018; Kaas, 1983) to assess the degree to which tactile signals are processed in CN. The picture that emerges is one in which CN plays an integral part in the transformation of tactile information as it ascends the neuraxis.

2.4 Results

To investigate tactile representations in CN, we measured the responses of individual CN neurons (n=33) to step indentations, sinusoidal skin vibrations (n=68), mechanical noise

(n=33), random dot patterns (n=31), and scanned bars (n=9). To compare CN responses to their peripheral counterparts, we simulated the spiking responses of tactile nerve fibers to the stimuli used in the CN recordings using a model that can reconstruct such responses with millisecond-level precision (Saal et al., 2017). To compare CN responses to their cortical counterparts, we analyzed previously collected cortical responses to analogous stimuli.

2.4.1 Adaptation properties of CN neurons reveal submodality convergence

Nerve fibers can be readily divided into two groups based on their responses to skin indentations: Slowly adapting type 1 (SA1) fibers respond throughout the skin indentation whereas rapidly adapting (RA) and Pacinian Corpuscle-associated (PC) fibers respond only to the onset and offset of the indentation and are silent during the intermediate sustained epoch (Pei et al., 2009). Examination of the responses of downstream neurons to skin indentations can thus reveal the sub-modality composition of their inputs. Specifically, responses during the sustained component reflect SA1 input, as only this class is active during this stimulus epoch; a strong phasic response during the offset of the indentation is indicative of RA or PC input, as only these two classes of nerve fibers produce an off response. Co-occurrence of these two response properties reflects convergent input from at least two classes of nerve fibers. In CN, we found that the responses of a majority of neurons comprise both sustained and off components, indicative of convergent input from multiple sub-modalities (Figure 2.1A).

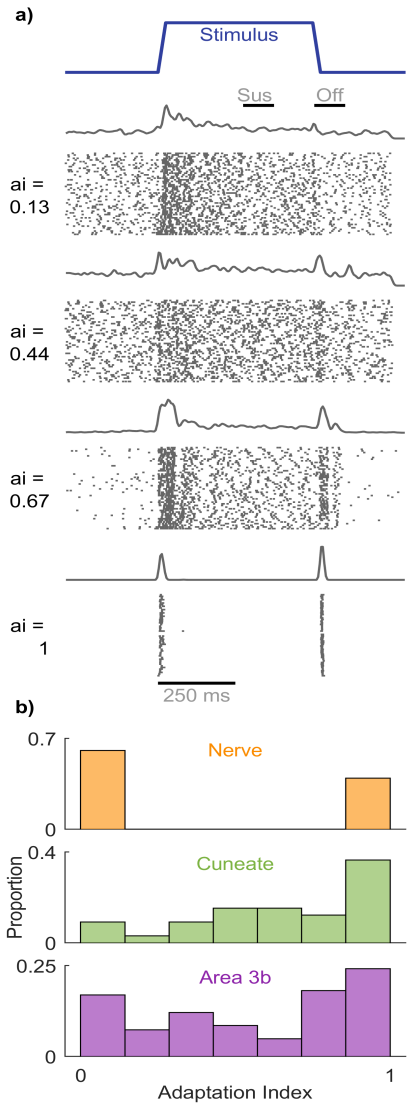

Figure 2.1: CN responses to step indentations. A| Responses of four CN neurons that span the range of convergence properties. B| AI index for the nerve (top), cuneate nucleus (middle), and the primary somatosensory cortex (bottom). AI segregates nerve fibers at the two extremes, whereas convergence is observed in both the CN and S1.

A previously developed 'adaptation index' (Pei et al., 2009) gauges the degree to which individual neurons receive convergent input from multiple cutaneous sub-modalities based on the relative strengths of the sustained and off responses. A value of 1 denotes RA-like responses (only an off-response, no sustained response), a value of 0 denotes SA1-like responses (only a sustained response, no off response), and an intermediate value denotes

convergent input (mixture of sustained and off responses). Adaptation indices computed on CN responses spanned the range from 0 to 1, with most falling between the two extremes, suggesting that convergence is the rule rather than the exception (Figure 2.1B). Indeed, the AI distribution of CN was more similar to that of S1 (KS-test, $D = 0.218$, $p = 0.19$) than that of the periphery (KS-test, $D = 0.545$, $p < 0.001$). A greater number of neurons exhibited pure RA-like than SA1-like responses, as has been found in S1, commensurate with the relative densities of these two groups of nerve fibers (RA/PC vs. SA1). To obtain a quantitative estimate of the proportion of multimodal neurons, we tested whether the firing rates during the sustained and offset periods were significantly different from the baseline period. Of the 33 neurons tested with skin indentations, 6% produced only sustained responses, 27% only offset responses, and 60% produced both sustained and offset responses (the remaining 7% only produced a transient onset response). Convergence of cutaneous sub-modalities is thus observed in a majority of neurons in CN.

2.4.2 CN responses to vibrations reveal submodality convergence

Next, we examined the responses of CN neurons to sinusoidal vibrations varying in amplitude and frequency, hoping to capitalize on the fact that different afferent classes exhibit different frequency sensitivity: SA1 fibers peak in sensitivity at low frequencies, PC fibers at high frequencies, and RA fibers at intermediate frequencies (Muniak et al., 2007; Talbot et al., 1968). We can then assess whether the frequency response characteristic of individual CN neurons resembles that of any single class of tactile nerve fiber or rather reflects convergent input from multiple fiber types. We found that some CN neurons respond exclusively to low frequencies, similar to SA1 fibers (Figure 2.2A), others to high frequencies, similar to PC fibers (Figure 2.2B), but many respond to the entire range of frequencies tested (Figure 2.2C), suggesting they receive convergent input from multiple tactile sub-modalities.

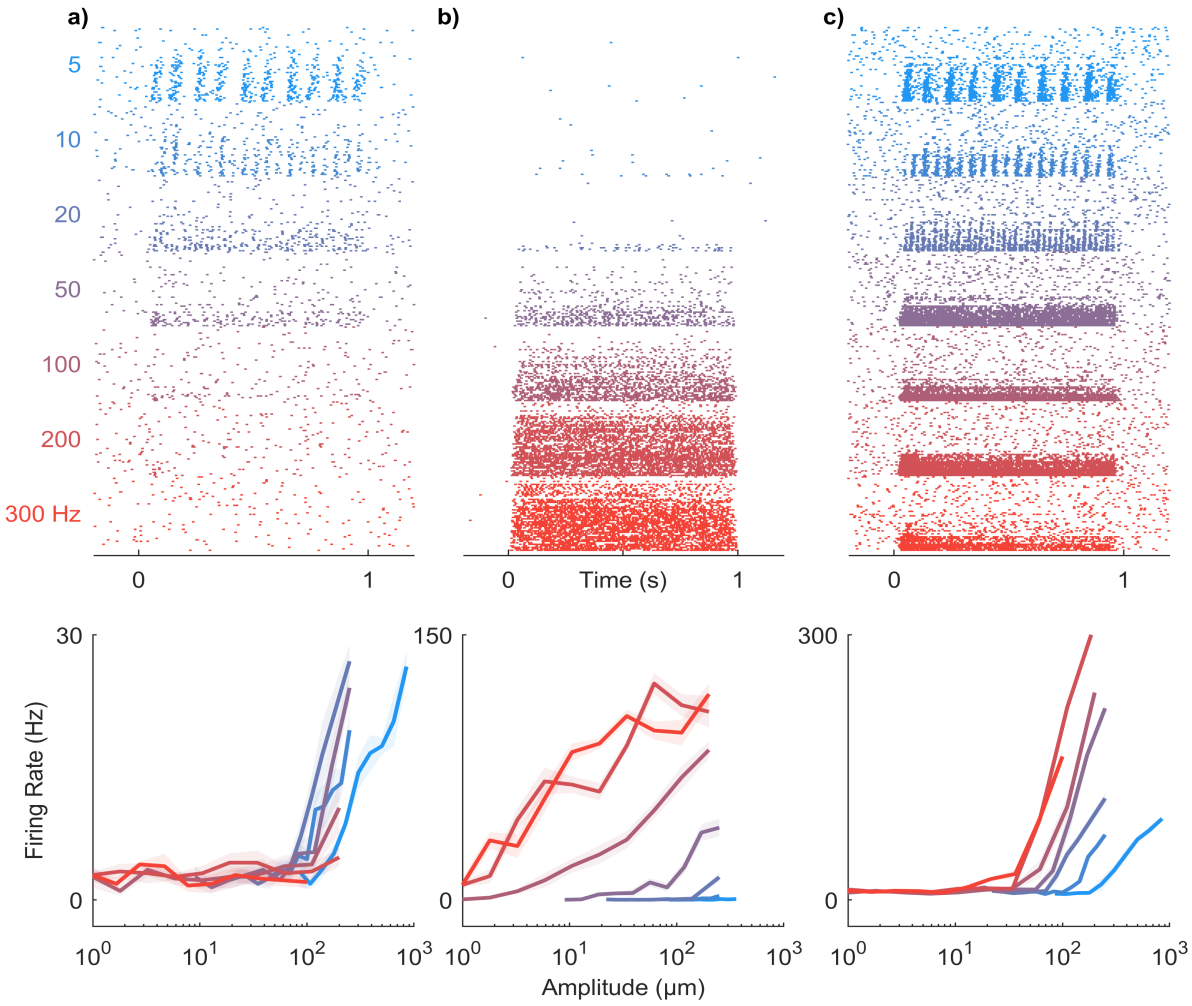

Figure 2.2: CN responses to vibrations. . A-C| Responses of three CN neurons to skin vibrations varying in frequency (from 5 to 300 Hz) and amplitude (1-1000 µm; ordered by frequency, then amplitude). Some CN neurons responded exclusively at low frequencies (A), others at high frequencies (B), but many CN neurons responded over a wider range of frequencies than does any one population of nerve fibers (C). As is the case in periphery and cortex, CN neurons often exhibited phase-locked responses to vibratory stimuli (see Supplemental Figure 2.1).

To quantitatively assess the contributions of different afferent classes to the responses of CN neurons, we regressed the firing rates of individual CN neurons onto the (simulated) population firing rates of nerve fibers from all three classes to a common set of vibrations (2.3A). First, we verified that the responses of most CN neurons could be well accounted

for using a linear combination of SA1, RA, and PC responses (mean $R^2 = 0.6$). Second, we assessed whether CN responses were better accounted for by multiple afferent classes than by one and found that, for most CN neurons, the cross-validated model fit increased significantly with the inclusion of all inputs (2.3A, mean ${R^2}_{\text{best}} = 0.50$, mean ${R^2}_{\text{all}} = 0.60$, mean $\Delta R^2 = 0.1$, ranksum = 5395, z = 3.2, p = 0.0013). We repeated the regression analysis on measured responses of tactile nerve fibers to similar sinusoidal vibrations to verify our ability to distinguish unimodal from multimodal responses. We found that measured afferent responses to vibrations were equally well accounted for with a single modality as they were multiple modalities (Figure 2.3A, mean ${R^2}_{\text{best}} = 0.83$, mean ${R^2}_{\text{all}} = 0.86$, mean $\Delta R^2 = 0.03$, ranksum = 1019, z = 1.53, p = 0.126). We found that 46% of CN neurons yielded ΔR^2 that were more than one standard deviation away from the mean R^2 obtained from nerve fibers, whereas only 10% of nerve fibers exceeded this threshold.

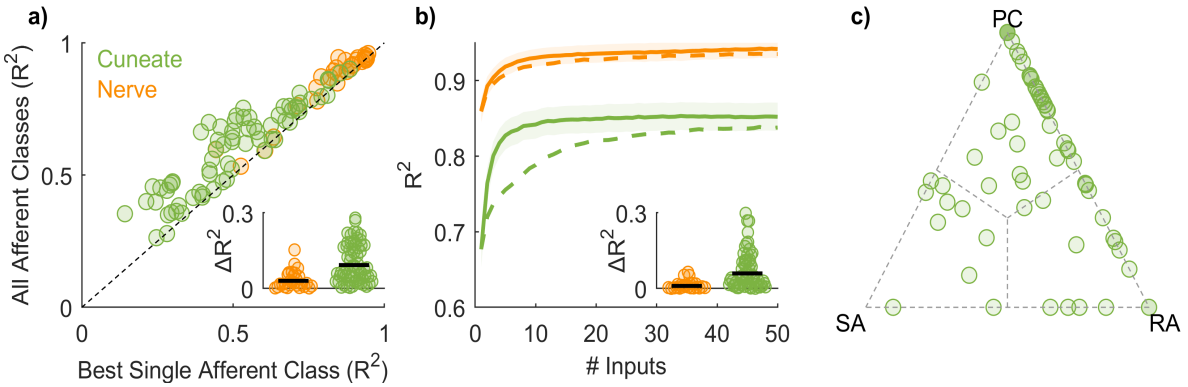

Figure 2.3: CN responses to vibrations reflect convergent input from multiple afferents, typically of multiple classes. A| Model fit with only one class of nerve fibers vs. model fit with multiple classes for CN and afferents. The responses of nerve fibers can be predicted nearly perfectly with a single afferent type whereas CN neurons often require multiple. Inset: model improvement when allowing all classes is significantly greater for cuneate than individual afferents. For this analysis, the mean response to each stimulus is used as a regressor, computed separately for each class of nerve fibers. B| Performance of regression models as a function of the number of afferents included in the analysis. Input from 2-5 nerve fibers is sufficient to achieve asymptotic performance for CN predictions, but only if convergence across sub-modalities is allowed. When only the best single afferent class is used (dashed line), an order of magnitude more afferents are required to reach asymptotic performance. Inset: At criterion, model performance is significantly improved when all afferent classes are included as regressors in models of CN responses. C| Normalized regression weights for each afferent class; each point corresponds to a CN neuron.

Third, we estimated the number of afferent inputs required to predict CN responses accurately. To this end, we simulated the responses of a population of nerve fibers and assessed our ability to predict the responses of individual CN neurons as we sequentially added simulated nerve fibers to the regression model (Figure 2.3B). We found that model fits typically leveled off (reached criterion performance) with just 2-5 inputs if all three classes of nerve fibers were included in the analysis. If only the most predictive afferent class was included, more inputs were required to achieve equivalent fits and performance plateaued at a lower level, consistent with the above analysis based on mean (simulated) population responses (Figure 2.3B – dashed line). Including all three afferent classes as regressors significantly improved CN predictions (mean $\Delta R^2 = 0.06$, ranksum = 5518, z = 3.07, p = 0.002). We validated the approach by verifying that including all three classes

did not improve afferent predictions (mean $\Delta R^2 = 0.01$, ranksum = 977, z = 0.90, p = 0.36). Examination of the optimized regression coefficients revealed that 15% of CN neurons were unimodal, 59% were bimodal, and the remainder (26%) were trimodal (Figure 2.3C). In conclusion, then, the responses of individual CN neurons to vibrations reflect input from multiple classes of nerve fibers so the submodality convergence observed in cortex is at least in part inherited from CN.

2.4.3 CN responses to vibrations reveal temporal computations

Neurons in somatosensory cortex have been shown to exhibit a variety of response properties to vibrations (Saal et al., 2015). Some neurons sum their inputs over time whereas others act as more complex temporal filters, comprising both excitatory and suppressive components. Examination of the rate-intensity functions for vibrations revealed suppressive components in the neuronal response (Supplementary Figure 2.1): Some CN neurons were always suppressed by vibration whereas others were excited by some vibrations and suppressed by others. For these neurons, regression models yielded significantly poorer fits when weights were constrained to be positive (mean 22% decrease). These suppressive components may constitute building blocks of more complex temporal feature filtering. To further characterize the process of temporal integration, we examined CN responses to mechanical noise. Specifically, we computed the mean response evoked in each afferent class immediately preceding each spike evoked in a given CN neuron (Figure 2.4). The resulting spike-triggered averages represent how a neuron integrates the signal from each population of nerve fibers. Some neurons simply summed their afferent input whereas others exhibited more complex response properties, with STAs that comprised excitatory and suppressive components, similar to those derived from S1 responses to analogous stimuli. As is the case in cortex, PC input tended to be more suppressive than was RA or SA1 input (Figure 2.4C). Temporal receptive fields that comprise excitatory and suppressive components confer to neurons a preference

to fluctuations in the afferent input; heterogeneity in the filters across neurons and input classes (Saal et al., 2015) gives rise to a high-dimensional representation of the input (Lieber and Bensmaia, 2019). From CN responses to mechanical noise, we also estimated the mean latency in CN to be around 10 ms (2.4D), approximately half of that in S1 ($\sim 18ms$).

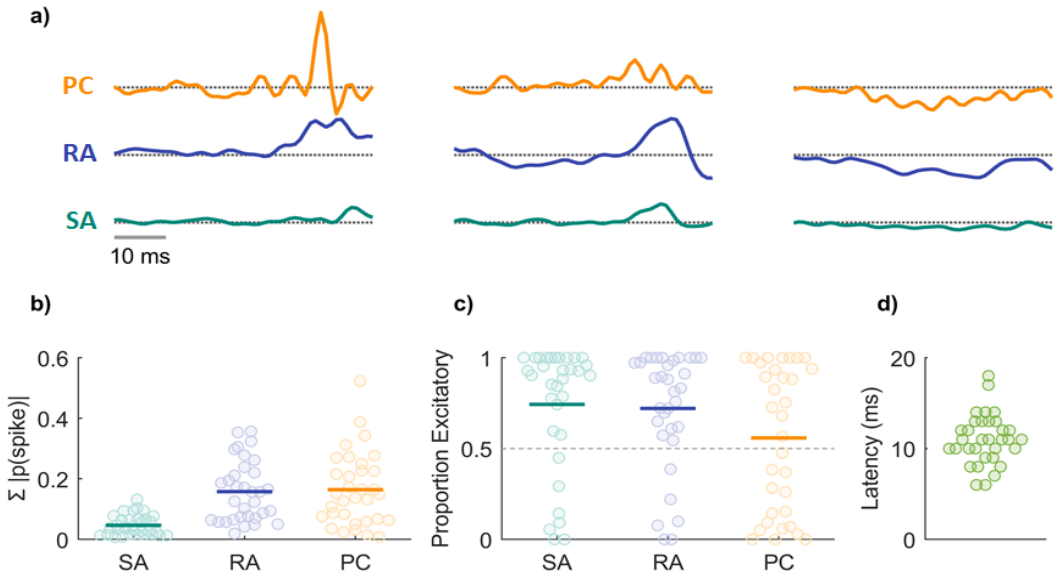

Figure 2.4: Temporal integration properties of CN neurons. A| Spike-triggered averages (STAs) computed from the responses of 3 CN neurons for inputs from the three classes of nerve fibers. STAs comprise both excitatory and suppressive components, as do their counterparts derived from the responses of S1 neurons. B| Summed absolute spike probability for each CN neuron with respect to afferent type. Given the frequency composition of the vibrations, the RA and PC drive was greater than was SA1 drive. C| Proportion of the afferent input that is excitatory vs suppressive. The temporal receptive fields of many CN neurons included both excitatory and suppressive components d— The latency, estimated from responses to mechanical noise, was about half of that in S1.

2.4.4 Spatial structure of CN receptive fields

Neurons in somatosensory cortex act not only as temporal filters (Saal et al., 2015) but also as spatial filters (Bensmaia et al., 2008; DiCarlo et al., 1998; Lieber and Bensmaia, 2019). The spatial receptive fields of S1 neurons comprise excitatory and inhibitory subfields, conferring to them a sensitivity to specific spatial features in their inputs. For example,

an elongated excitatory subfield flanked by an inhibitory one will confer to a neuron a selectivity for orientation (Bensmaia et al., 2008; Hubel and Wiesel, 1962). With this in mind, we reconstructed the spatial receptive fields of CN neurons from their responses to random patterns of embossed dots scanned across the skin (DiCarlo et al., 1998; Lieber and Bensmaia, 2019). First, we found that the RFs of CN neurons tend to be larger than are those of SA1 or RA fibers (Johnson and Lamb, 1981), as expected given the inferred convergence of afferent input onto individual CN neurons (Figure 2.5A&B). Second, CN neurons have marginally smaller RFs than do their cortical counterparts (Figure 2.5B&D), as expected given their relative positions along the neuraxis. The mean RF size is 7.2 mm2 in CN and 9.9 mm2 in cortex (t-test: $t(44) = 2.8$, $p = 0.072$). Third, CN neurons have complex RFs, often comprising excitatory and inhibitory subfields, like their cortical counterparts (Figure 2.5A&C). As in cortex, the excitatory subfields of CN neurons tend to be larger than their inhibitory counterparts. However, CN RFs tend to comprise a greater number of distinct subfields than do their S1 RFs (mean of 4 vs. 2.1 mm2, $t(44) = 4$, $p < 0.001$). While the excitatory masses are similar in CN and S1, the inhibitory masses are smaller in CN than in S1 (excitatory: 5.6 vs. 6.6 mm^2, $t(44) = 1.37$, $p = 0.178$; inhibitory: 1.5 vs. 3.3 mm^2, $t(44) = 2.8$, $p < 0.008$). Nonetheless, the spatial structure of the receptive fields observed in CN is qualitatively similar to its counterpart in S1.

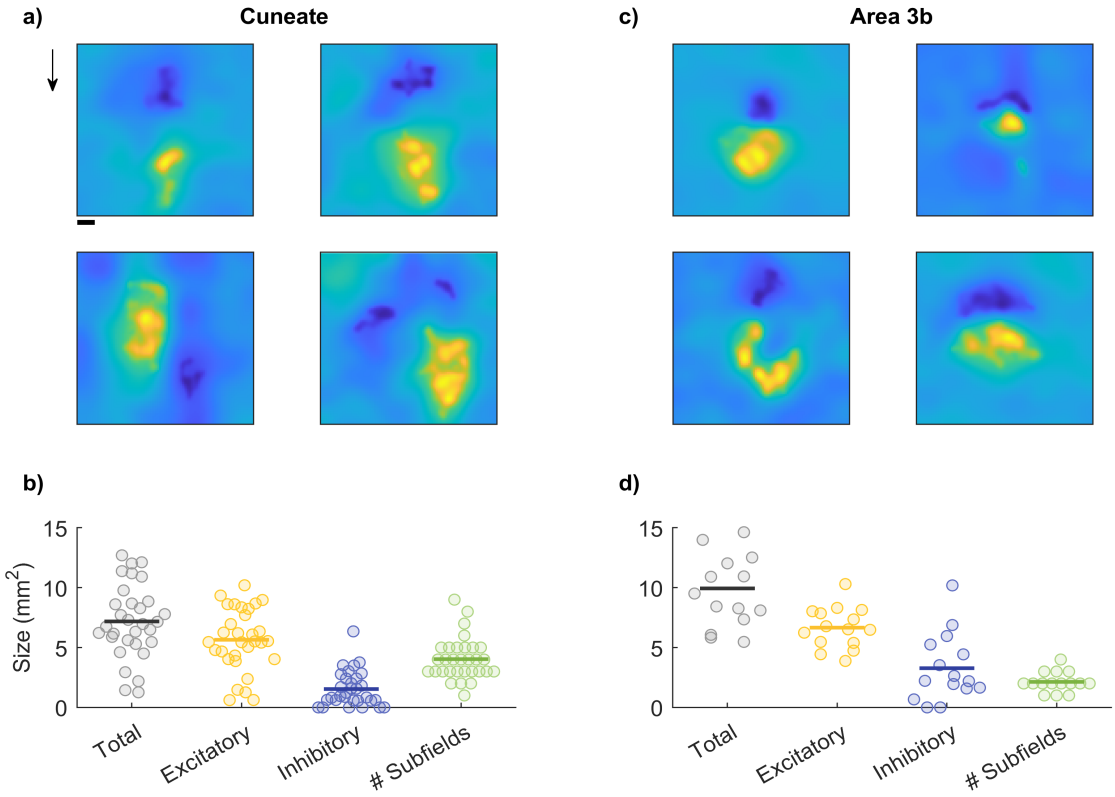

Figure 2.5: Spatial receptive fields of CN neurons. A| Reconstructed receptive fields for 4 cuneate neurons. RFs typically comprise both excitatory and inhibitory subfields in a variety of conformations. Cuneate RFs are similar to their S1 counterparts (panel C). Arrow indicates the direction in which the dot pattern was scanned. Scale bar is 1mm. B| Cuneate receptive fields are on average smaller than those in S1 (panel D), a difference that is primarily driven by smaller inhibitory subfields.

2.4.5 CN neurons exhibit feature selectivity

Next, we examined whether the spatial structure of RFs confer to the firing rate responses of CN neurons a selectivity for specific geometric features, as it does in cortex but not the periphery. To this end, we measured the responses of CN neurons to oriented edges scanned across their RFs. We found that the firing rates of a subset of CN neurons are modulated by orientation, (Figure 2.6A, Supplementary Figure 2.2), responding more strongly to edges at some orientations than others. Some neurons are also modulated by direction of movement, responding strongly to a bar scanned in one direction but less so to the same bar scanned

in the opposite direction (top right and bottom left neurons in Figure 2.6A). We quantified the strength of the orientation tuning using a metric – the orientation selectivity index – that takes on a value of 1 when a neuron responds only to a single orientation and 0 when it responds uniformly to all orientations. The degree of orientation selectivity in CN is intermediate between that seen in the nerve – where none exists – and in cortex (Figure 2.6B). Therefore, the feature selectivity observed in cortex is to some extent inherited from its inputs.

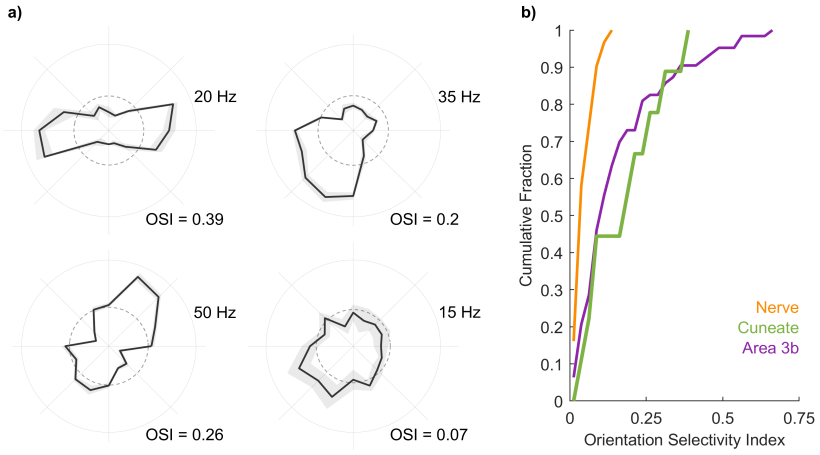

Figure 2.6: Orientation tuning in CN neurons. A| Response of example CN neurons to oriented edges. The angular coordinate denotes orientation, the radial coordinate denotes firing rate, and the dashed circle denotes the firing rate averaged across conditions. B| Cumulative distribution of orientation selectivity index derived from the responses of nerve fibers, CN neurons, and S1 neurons. CN responses are more strongly tuned for orientation than are nerve fibers but more weakly tuned than are the some S1 neurons.

2.5 Discussion

The objective of the present study was to characterize the tactile representation in CN and to assess the degree to which CN responses reflect computations on their inputs. To these ends, we probed CN responses using stimuli whose representation in the peripheral nerve has been extensively characterized, allowing us to disentangle derived response properties from those inherited from the inputs. Any difference between nerve and CN responses could

then be attributed to computations within CN (or possibly to an intervening synapse in the spinal cord (Abraira and Ginty, 2013; Giesler et al., 1984; Liao et al., 2015; Loutit et al., 2021)). We found that CN neurons receive convergent input from multiple tactile submodalities, exhibit spatial and temporal filtering properties that had previously been attributed to cortical processing, and are tuned for behaviorally relevant object features. Comparison of CN responses to their upstream and downstream counterparts suggests that the tactile representation in CN is more similar to its counterpart in cortex than it is to that in the nerve.

2.5.1 Submodality convergence

Tactile nerve fibers that innervate the glabrous skin of monkeys can be divided into three clearly delineated classes, each with distinct response properties (Delhaye et al., 2018). While each sub-modality might be more responsive to any one stimulus feature, information about most features is distributed over all three sub-modalities and the resulting perceptual experience reflects this integration (Lieber et al., 2017; Muniak et al., 2007; Saal and Bensmaia, 2014; Weber et al., 2013). As might be expected, then, the responses of individual S1 neurons typically reflect convergent input from multiple classes of nerve fibers (Pei et al., 2009). Where this integration might first take place was unclear, however. Studies with cats suggested a lack of submodality convergence in CN (Bystrzycka et al., 1977; Douglas et al., 1978; Ferrington et al., 1987; Gynther et al., 1995; Vickery et al., 1994) whereas studies in rodents conclude that the trigeminal nucleus – a structure analogous to the CN that receives inputs from the face – exhibits submodality convergence at the single cell level (Kaloti et al., 2016; Minnery et al., 2003; Sakurai et al., 2013). Here, we show that the CN of primates features submodality convergence. Indeed, the majority of CN neurons produce both an SA1-like sustained response to the static component of a skin indentation and an RA/PC-like phasic response at the offset of the indentation. Furthermore, individual CN

neurons tend to respond to a wider range of frequencies than do primary afferents of any one class. The submodality convergence observed in somatosensory cortex is thus, at least in part, inherited from its inputs and begins at the earliest processing stage along the dorsal column-medial lemniscus pathway.

2.5.2 Neural computations

Tactile nerve fibers have small RFs that consist of one or more excitatory hotspots (Johansson, 1978; Vega-Bermudez and Johnson, 1999) and faithfully encode local skin deformations (Saal et al., 2017). In contrast, S1 neurons have larger RFs that comprise excitatory and inhibitory subfields (Bensmaia et al., 2008; DiCarlo et al., 1998; Lieber and Bensmaia, 2019), which confer to them a selectivity for spatial features in their inputs. Individual cortical neurons also act as temporal filters (Saal et al., 2015), which confers to them a selectivity for temporal features in their inputs. The idiosyncratic spatial and temporal filtering properties of individual S1 neurons give rise to a high-dimensional representation of the input in somatosensory cortex, in which different features of grasped objects are simultaneously and unambiguously encoded (Bensmaia et al., 2008; DiCarlo et al., 1998; Lieber and Bensmaia, 2019, 2020; Pei et al., 2010).

Here we show that the spatial and temporal computations observed in cortex are also observed in CN. First, the spatial RFs of CN neurons comprise excitatory and inhibitory subfields and, while somewhat smaller (as expected since CN is upstream from cortex), resemble their cortical counterparts. Second, individual CN neurons process time-varying inputs in a variety of different ways – ranging from integration to differentiation – that are analogous to their cortical counterparts. CN thus contributes to the processing of sensory information and CN neurons exhibit response properties that are qualitatively similar to their counterparts in S1.

2.5.3 Feature selectivity

The spatiotemporal response properties of S1 neurons confer to them a preference for certain stimulus features. For example, individual S1 neurons exhibit a selectivity for the direction in which objects move across the skin (Gardner and Costanzo, 1980; Pei et al., 2010) or idiosyncratic preferences for different surface textures (Lieber and Bensmaia, 2019). Another well-documented feature selectivity in S1 is for oriented edges: a large proportion of S1 neurons respond preferentially to edges at a specific orientation (Bensmaia et al., 2008). This orientation selectivity is attributed to the neuron's RF structure, which comprises excitatory and inhibitory subfields, analogous to neurons in primary visual cortex (Hubel and Wiesel, 1962). We show that CN neurons also exhibit orientation selectivity, suggesting that some of the feature selectivity observed in S1 is inherited from its inputs.

Feature extraction results in a sparsening of the stimulus representation, which can result in an overall loss of information (Babadi and Sompolinsky, 2014), unless it is accompanied by an expansion of the size of the neuronal population (Daniel and Whitteridge, 1961). Not surprisingly, the CN is estimated to comprise three to five times more neurons than there are nerve fibers that innervate the corresponding dermatomes, with a preferential expansion of the representation of the hand (Biedenbach, 1972; Corniani and Saal, 2020; Darian-Smith and Ciferri, 2006; Xu and Wall, 1999), also reflected in S1 (Corniani and Saal, 2020), and consistent with observations in other animals (Catania et al., 2011; Lehnert et al., 2021; Wassle et al., 1990). Thus, the expanded neuronal representation in CN is consistent with its role in feature extraction.

2.5.4 Processing along the medial leminiscal pathway

Thus far we have shown that CN plays an active role in the processing of tactile information. Furthermore, it is likely that the dorsal column nuclei are the first node at which cortical magnification occurs (Lehnert et al., 2021). Given this, it must be presumed that the

primary thalamic nuclei (specifically the ventroposterior lateral nucleus – VPL), another structure that is often overlooked, builds on top of the outputs of CN, performing further computations and perhaps magnification, and then projects to S1. The degree to which the functions and computations of CN and VPL are distinct is unknown, as is the purpose of top-down modulation on each structure. Conclusions The naïve textbook story is that CN is a simple relay station that does not effect any computations on its inputs but rather transmits them unprocessed. The putative role of CN, if any, has been to provide an opportunity to modulate the gain of the afferent input depending on its behavioral relevance via top down signals (Berkley et al., 1986; Conner et al., 2021). We show that, in addition to this gain modulation, the responses of CN neurons reflect a significant transformation of their afferent inputs, conferring to them properties that were heretofore attributed solely to cortex. CN is thus an active contributor to the process by which ambiguous signals from the periphery are converted into sensory representations that support robust and meaningful percepts and guide behavior.

2.6 Methods

2.6.1 Neurophysiology

Animals & surgical preparation

Neuronal responses were obtained from 7 rhesus macaques (5 males and 2 females, 4-14 years of age, 4-12 kg). Monkeys were anesthetized and placed in a stereotaxic frame with their neck flexed at 90 degrees to provide access to the dorsal brainstem. The foramen magnum was exposed and the inferior aspect of the occipital bone was removed. The dura above obex was resected to reveal the brainstem. All surgical procedures were approved and monitored by the Institutional Animal Care and Use Committee and were consistent with federal guidelines. The neurophysiological methods for the cortical and nerve fiber

responses have been previously described (Bensmaia et al., 2008; Harvey et al., 2013; Pei et al., 2009). Anesthesia undoubtedly effects our results in a fundamental manner as the top-down modulation of CN by cortex is absent under anesthesia (Andersen et al., 1962; Suresh et al., 2017). Nevertheless, our study focuses on the feed-forward processing capacity of CN neurons and these canonical properties are unlikely to change during consciousness.

Neurophysiological recordings

Neuronal activity was monitored using 16-channel linear probes (V-Probe, Plexon, Dallas, TX) and amplified and stored using a Cerebus system (Blackrock Microsystems, Salt Lake City, Utah). Probes were positioned with a stereotaxic system, using the obex as a landmark to locate the CN. Units with receptive fields on the glabrous surface of the hand were isolated. Responses from 143 neurons were obtained across experimental conditions. Hand mapping revealed that the majority of isolated units had small receptive fields, confined to a single digit pad or palmar whorl, with the exception of neurons that exhibited PC-like responses.

Anesthesia

All animals were induced with a combination of ketamine, dexmedetomidine, and buprenorphine. Isoflurane (1-2%) was then delivered continuously via inhalation and decreased during the neurophysiological recordings. While anesthesia can have a profound impact on neural responses (Calancie et al., 1991; Cheung et al., 2001; Noda & Takahashi, 2015; Sellers et al., 2015; Shumkova et al., 2021), several observations suggest that the CN recordings were only minimally impacted. First, the impact of anesthesia tends to be more pronounced in cortex (Michael et al., 2008). Given that CN is the first recipient of afferent input, itself minimally affected by anesthesia (Cheng et al., 2013), the impact of anesthesia on CN responses, at least those driven by peripheral input, is likely minimal. Second, certain anesthetics have been shown to affect the temporal response properties of neurons in cortex (Cheung et al.,

2001). That we observe precise and repeatable phase-locking of CN responses to vibrations (2.1C) suggests that the anesthesia did not affect the temporal precision of the responses. Third, CN has been shown to receive projections from cortex (Conner et al., 2021; Berkley et al., 1986) and this top-down drive is almost certainly abolished or at least strongly altered under anesthesia. Note, however, the cortical modulation of cutaneous responses in CN seems to be primarily suppressive (Conner et al., 2021) under conditions where this input may be disruptive (He et al., 2019). The similarity between the responses of CN neurons under anesthesia and those of S1 neurons monitored in awake animals implies that CN responsivity is relatively unaffected by anesthesia. Finally, in a previous series of experiments described in (Kuresh et al., 2017), we recorded responses of three CN neurons to sinusoidal vibrations and found that vibratory thresholds were qualitatively similar (Supplementary Figure 2.3).

2.6.2 Tactile stimulation

We presented five classes of stimuli – skin indentations, sinusoidal vibrations, band-pass mechanical noise, scanned random dot patterns, and scanned edges – each with precisely controlled speed, force, frequency, and/or amplitude. In some cases, multiple stimulus classes were delivered while recording from a given neuron. Indentations, sinusoids, and noise stimuli were delivered with a probe (diameter = 1 mm) driven by a custom shaker motor (Westling et al., 1976), pre-indented 0.5 mm into the skin. Scanned random dots and edges were presented using a miniaturized version of the drum stimulator (Lieber and Bensmaia, 2019; Weber et al., 2013). Edges were presented using a custom-stimulator that can scan stimuli across the skin in different directions and whose third degree of freedom allows for indentation into and retraction from the skin (see (Pei et al., 2014)). Responses to skin indentation and sinusoids were collected from 4 monkeys (number of neurons = 33, 68 respectively), responses to bandpass noise and random dot patterns from 2 monkeys (n = 33, 31), and responses to

edges from 1 monkey (n = 9).

Skin indentations

The amplitude of the ramp and hold indentation was 1 mm and their overall duration was 0.5 seconds, with on- and off- and ramps lasting 25 ms, and separated by a 0.5-s interval. Indentations were presented 100 times.

Sinusoids

Sinusoidal vibrations were delivered at 7 frequencies (5-300 Hz) and 10 amplitudes, which spanned the achievable range at each frequency, given the limitations of the stimulator. Each frequency-amplitude combination, lasting 1 s, was presented 5 times in pseudorandom order, separated by a 1-s interstimulus interval, for a total of 350 trials.

Bandpass mechanical noise

White Gaussian noise was filtered with different high and low pass frequencies (low: 5-50 Hz, high: 10-200 Hz) to yield 10 unique stimuli (as previously described in (Muniak et al., 2007), each lasting 1 s and separated by a 0.3-s interval.

Scanned random dot patterns

Random dot patterns were printed (Form 2, Formlabs, Somerville, MA) on a drum (2.5-in diameter) using previously used geometries and densities (DiCarlo et al., 1998; Lieber and Bensmaia, 2019). Patterns were repeatedly scanned across the skin at 80 mm/s. For the first scan, the edge of the pattern was aligned with the estimated the center of the receptive field and indented into the skin by 0.5 mm. For each of 100 subsequent scans, the drum was progressively translated by 0.4 mm along the axis perpendicular to the axis of rotation.

Scanned edges

An edge (1-mm high, 1-mm wide, 0.25-mm chamfer) was printed on a miniature drum, whose rotation was driven by a rotational motor. The orientation of the drum on the skin was controlled by a second rotational motor. A third motor controlled the vertical excursion of the drum and allowed for it to be lifted in between changes in orientation. The edge was scanned five times at 80 mm/s at each of 16 orientations (0 – 337.5 degrees with a 22.5 degree spacing).

2.6.3 Data analysis

Adaptation index

The adaptation index (Pei et al., 2009) indicates the relative firing rate of the sustained and offset periods. SA1 afferents respond to the onset and sustained period while RA and PC afferents respond to the onset and offset transient periods. Thus, the submodality composition of the inputs of a downstream neuron can be measured by taking the ratio of the offset and sustained period. The baseline firing rate was subtracted from both the computed sustained frsus and offset froff firing rates (measured between 0.275-0.375 and 0.505-0.605 seconds respectively). The adaptation index was then computed as:

$$ai = |tan^{-1}(\frac{fr_{off}}{fr_{sus}}) * \frac{2}{\pi}|$$

Afferent convergence

Given that each class of nerve fibers exhibits a unique frequency response characteristic, we sought to determine if the cuneate responses could be explained by linear combinations of inputs from the three afferent classes. To this end, we simulated the responses of each afferent type to the sinusoidal stimuli used in this study. For this, we used TouchSim, a model that

yields millisecond precision reconstructions of the responses of every tactile nerve fiber that innervates the glabrous skin of the hand to arbitrary stimuli delivered to the skin (Saal et al., 2017). The firing rates evoked by each stimulus was then averaged across afferents of the same type. For each cuneate neuron, we used linear regression in the form:

$$fr_{on} = \varphi_0 + \varphi_1 fr_{SA1} + \varphi_2 fr_{ra} + \varphi_3 fr_{pc}$$

We compared the performance of the full model to that of models that only included one class of nerve fibers. We assessed model performance using 5-fold cross-validation to ensure that models with more parameters did not outperform simpler models due to overfitting. We then compared the best performing single afferent model to that of the full model for each neuron. To estimate the number of afferents that contribute to the CN response, we performed a regression analysis using the firing rates of individual nerve fibers as regressors. We then used an stepwise linear regression process to determine the optimal combination of inputs. Briefly, on the first iteration, we selected the nerve fiber that had the highest correlation with the CN response. During each subsequent step, we measured the increase in correlation when adding every other afferent in the population, either across classes or within class. We then incorporated the fiber that most improved the regression performance. We proceeded until the addition of an additional regressor failed to improve the model fit more than 5%. To determine the relative contributions of each afferent type to the CN response, we summed the absolute regression coefficient within afferent type and normalized by the summed absolute regression values across afferent types.

Spike-triggered average - transfer function

Responses to mechanical noise can be used to estimate the transfer function of a neuron (Saal et al., 2015; Schwartz et al., 2006). Accordingly, we simulated the responses of all

the nerve fibers that innervate the glabrous skin of the hand to the bandpass mechanical noise used in the neurophysiological experiments and averaged their responses across fibers of each class. We then performed a spike triggered average (STA) (Schwartz et al., 2006) of the response of each afferent conditioned on each spike in CN. That is, the response of each afferent population over the 100 ms preceding each CN spike was averaged across CN spikes. The resulting filter was smoothed using a Gaussian filter (sd = 5 ms) and the baseline firing rate was subtracted. We then standardized the resultant filter for each cuneate-afferent pair with respect to the period between 100 and 50 ms before the cuneate spike, which we expect to reflect noise. We then thresholded (Z $>$ 2) the Z-scored probabilities and computed the magnitude and width of the filters.

Harmonic ratio

To determine the extent to which CN response to sinusoids were phase-locked, we computed the harmonic ratio of the response to each stimulus. Excluding responses with fewer than 5 spikes, we performed a Fast Fourier transform (FFT) of the peristimulus spike histogram (binned at 1/5f;), averaged the mean amplitude at the fundamental frequency (Af) and its first harmonic (Ah1), and divided the resulting value by the median amplitude across all frequencies ($\tilde{\text{A}}$):

$$hr = \frac{(A_f + A_{h1})/2}{\tilde{A}}$$

where

$$A = |real[FFT(x)] + imag[FFT(x)]| * 1/fs$$

We repeated this analysis for Poisson spike trains to obtained a distribution of harmonic ratios obtained by chance.

Spatial receptive fields

We used standard techniques to estimate the spatial receptive field of each cuneate neuron (cf. (DiCarlo et al., 1998; Lieber and Bensmaia, 2019)). In brief, we averaged the 16 mm x 16 mm swath of the random dot pattern that impinged on the skin at the time of each cuneate spike. To remove the curvature of the drum reflected in the resulting STA, we subtracted a 2nd order polynomial plane from it. The resultant STA was then standardized and thresholded to isolate excitatory and inhibitory lobes. To identify the number of subfields for cortical and cuneate receptive fields, we fitted 2D Gaussians to each RF. Each Gaussian subfield had the following form:

$$G(x, y) = a \cdot e^{(-\frac{1}{2}(L\Sigma^{-1}L^T))}$$

where L=[x-$\mu_x, y - \mu_y$], $\Sigma = CovMat(\sigma_x, \sigma_y, \theta)$, a is the amplitude (a $>$ 0 denotes an excitatory patch, a $<$ 0 an inhibitory one), (x, y) denote the medial-lateral and proximal-distal locations on the skin surface, respectively, (μ_x, μ_y) represent the center of the Gaussian, (σ_x, σ_y) its standard deviations along the two axes, and θits orientation. Therefore, every RF is described by a total of N$\times$6 parameters (6 parameters for each Gaussian component: a, $\mu_x, \mu_y, \sigma_x, \sigma_y$, and θ; and N Gaussian components). Nonlinear least-squares optimization was used to find the best parameters. N represents the minimum number of Gaussian subfields needed to achieve R2 $>$ 0.9 of 90% of the maximum achievable R^2.

Orientation tuning

Spiking responses evoked at each orientation were aligned to a reference stimulus trace consisting of 6 Gaussians spaced according to the stimulus speed. The spike rate evoked by the stimulus, centered around the peak response, was averaged over a window of 314 ms, corresponding to 6.2 mm of travel (5% of a complete rotation of the drum), though the

window size did not affect the results over a wide range (Supplementary Figure 2.2). The tuning of each neuron was gauged using an Orientation Selectivity Index, given by:

$$OSI = \sqrt{\frac{\Sigma(R_\varphi * sin(2\varphi))^2 + (R_\varphi * cos(2\varphi))^2}{\Sigma R_\varphi}}$$

Where is the orientation of the stimulus and R is the firing rate at that orientation. Reliability of the OSI was tested using a permutation test, for which neural responses were shuffled 10000 times and the OSI recomputed.

2.6.4 Supplementary Figures

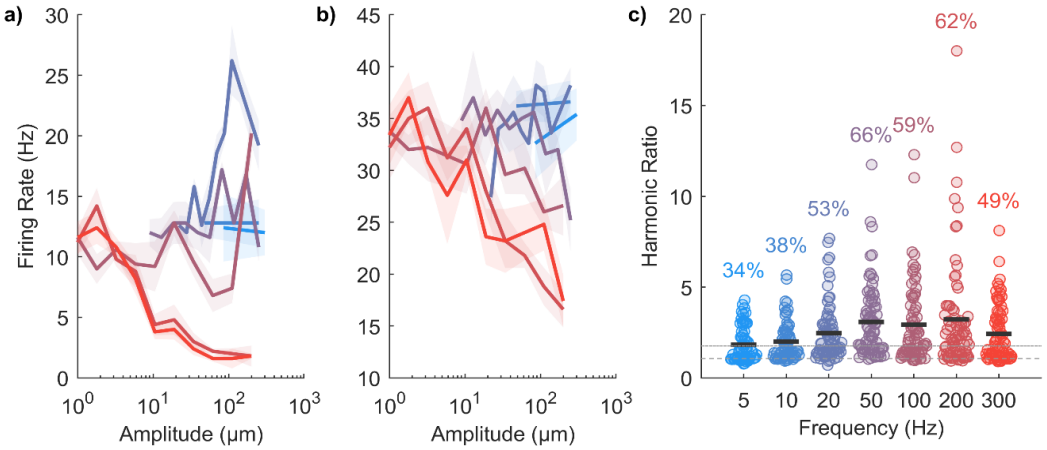

Supplementary Figure 2.1: Frequency characteristics of CN neurons. A&B| Example rate-intensity plots for two CN neurons. The neuron in panel A is sometimes excited, sometimes inhibited by skin vibrations depending on their frequency while the neuron in panel B exhibits only suppression. C| The proportion of neurons that are significantly tuned to each frequency. The dashed line indicates the mean harmonic ratio of a Poisson neuron (~ 1), $and the dotted line above is the value 3 standard deviations above the mean.$

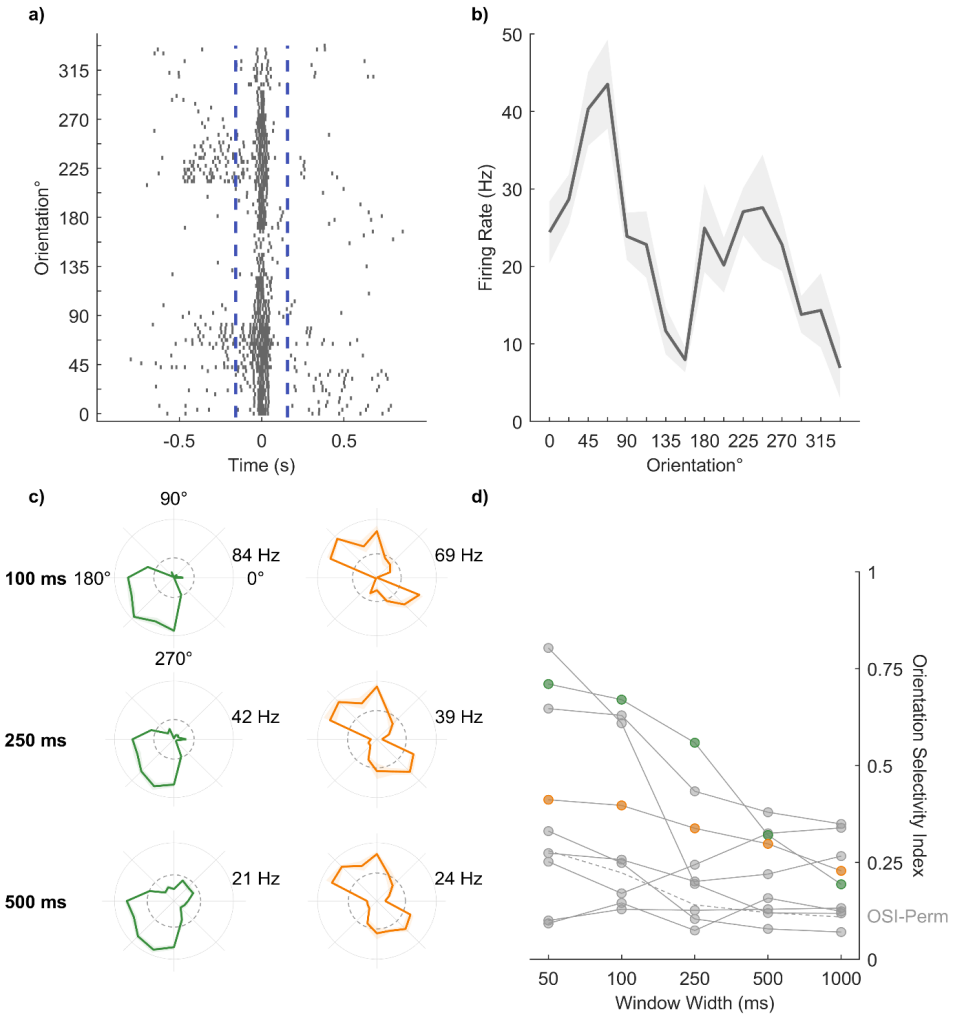

Supplementary Figure 2.2: Orientation tuning is stable with respect to window size. A| Raster plot of the responses of an example CN neuron to edges at each orientation aligned to the peak response. B| Tuning curve for the neuron shown in panel A. C| Polar plots for 2 example neurons computed from the responses averaged over 3 time windows. D| Vector strength for all neurons computed over different windows. Example neurons from panel C are highlighted in the corresponding color. OSI-Perm indicates the orientation index averaged across neurons when the firing rates are shuffled across trials.

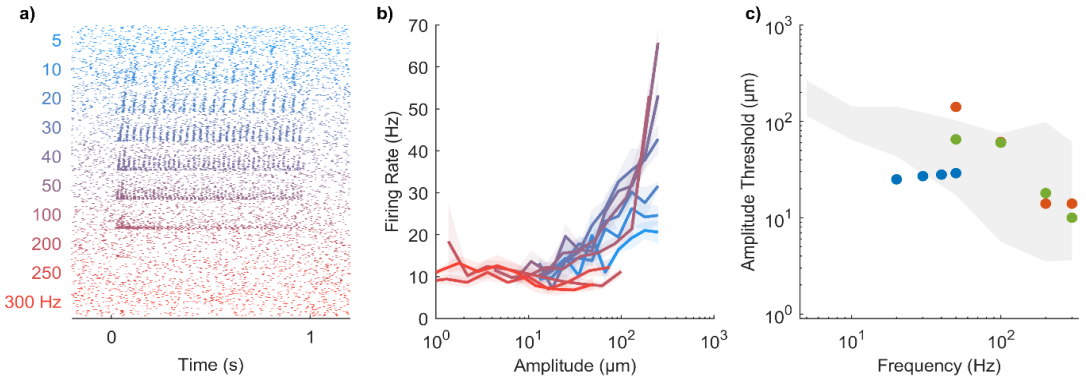

Supplementary Figure 2.3: Vibrotactile responses are minimally altered by anesthesia. A| Example raster and B| rate-intensity function for a neuron recorded from an awake monkey with a chronic array. C| Thresholds derived from the responses of three neurons measured in awake monkeys were similar to their counterparts measured under anesthesia. For two neurons (denoted by green and orange dots), the vibratory stimuli were delivered using a different vibratory stimulator (mini shaker, 4810, Bruel and Kjaer, Naerum, Denmark). For all three neurons, the contactor was smaller (1 mm) than that used in the acute experiments. The gray outline shows the range of thresholds observed for anesthetized monkeys while dots indicate the thresholds for the units monitored in awake monkeys.

2.7 References

J. M. Goodman, S. J. Bensmaia, "The Neural Mechanisms of Touch and Proprioception at the Somatosensory Periphery" in The Senses, (Elsevier, 2020).

R. S. Johansson, Tactile sensibility in the human hand: receptive field characteristics of mechanoreceptive units in the glabrous skin area. The Journal of Physiology 281, 101–125 (1978).

W. H. Talbot, I. Darian-Smith, H. H. Kornhuber, V. B. Mountcastle, The sense of flutter-vibration: comparison of the human capacity with response patterns of mechanoreceptive afferents from the monkey hand. Journal of Neurophysiology 31, 301–334 (1968).

J. Hyvärinen, A. Poranen, Receptive field integration and submodality convergence in the hand area of the post-central gyrus of the alert monkey. The Journal of Physiology 283, 539–556 (1978).

J. D. Lieber, S. J. Bensmaia, High-dimensional representation of texture in somatosensory

cortex of primates. Proceedings of the National Academy of Sciences of the United States of America 116, 3268–3277 (2019).

Y.-C. Pei, P. V. Denchev, S. S. Hsiao, J. C. Craig, S. J. Bensmaia, Convergence of submodality-specific input onto neurons in primary somatosensory cortex. Journal of neurophysiology 102, 1843–1853 (2009).

H. P. Saal, S. J. Bensmaia, Touch is a team effort: interplay of submodalities in cutaneous sensibility. Trends in Neurosciences 37, 689–697 (2014).

S. J. Bensmaia, P. V. Denchev, J. F. Dammann, J. C. Craig, S. S. Hsiao, The representation of stimulus orientation in the early stages of somatosensory processing. The Journal of Neuroscience 28, 776–786 (2008).

J. J. DiCarlo, K. O. Johnson, S. S. Hsiao, Structure of receptive fields in area 3b of primary somatosensory cortex in the alert monkey. The Journal of neuroscience: the official journal of the Society for Neuroscience 18, 2626–45 (1998).

H. P. Saal, M. A. Harvey, S. J. Bensmaia, Rate and timing of cortical responses driven by separate sensory channels. eLife 4, e10450 (2015).

E. Bystrzycka, B. S. Nail, M. Rowe, Inhibition of cuneate neurones: its afferent source and influence on dynamically sensitive 'tactile' neurones. The Journal of Physiology 268, 251–270 (1977).

C. Ebert, K. Bagdasarian, S. Haidarliu, E. Ahissar, A. Wallach, Interactions of Whisking and Touch Signals in the Rat Brainstem. J Neurosci 41, 4826–4839 (2021).

H. Jörntell, et al., Segregation of Tactile Input Features in Neurons of the Cuneate Nucleus. Neuron 83, 1444–1452 (2014).

A. S. Kaloti, et al., Representation of Stimulus Speed and Direction in Vibrissal-Sensitive Regions of the Trigeminal Nuclei: A Comparison of Single Unit and Population Responses. PLOS ONE 11, e0158399 (2016).

C. L. Witham, S. N. Baker, Modulation and transmission of peripheral inputs in monkey

cuneate and external cuneate nuclei. Journal of Neurophysiology 106, 2764–2775 (2011).

J. M. Conner, et al., Modulation of tactile feedback for the execution of dexterous movement. bioRxiv, 2021.03.04.433649 (2021).

B. P. Lehnert, et al., Mechanoreceptor synapses in the brainstem shape the central representation of touch. bioRxiv, 2021.02.02.429463 (2021).

B. P. Delhaye, K. H. Long, S. J. Bensmaia, Neural Basis of Touch and Proprioception in Primate Cortex. Compr Physiol 8, 1575–1602 (2018).

J. H. Kaas, What, if anything, is SI? Organization of first somatosensory area of cortex. Physiological Reviews 63, 206–231 (1983).

H. P. Saal, B. P. Delhaye, B. C. Rayhaun, S. J. Bensmaia, Simulating tactile signals from the whole hand with millisecond precision. Proceedings of the National Academy of Sciences of the United States of America 114, E5693–E5702 (2017).

M. A. Muniak, S. Ray, S. S. Hsiao, J. F. Dammann, S. J. Bensmaia, The Neural Coding of Stimulus Intensity: Linking the Population Response of Mechanoreceptive Afferents with Psychophysical Behavior. J. Neurosci. 27, 11687–11699 (2007).

D. H. Hubel, T. N. Wiesel, Receptive fields, binocular interaction and functional architecture in the cat's visual cortex. The Journal of Physiology 160, 106–154 (1962).

K. O. Johnson, G. D. Lamb, Neural mechanisms of spatial tactile discrimination: neural patterns evoked by braille-like dot patterns in the monkey. J Physiol 310, 117–144 (1981).

V. E. Abraira, D. D. Ginty, The Sensory Neurons of Touch. Neuron 79, 618–639 (2013).

G. J. Giesler, R. L. Nahin, A. M. Madsen, Postsynaptic dorsal column pathway of the rat. I. Anatomical studies. J Neurophysiol 51, 260–275 (1984).

C.-C. Liao, G. E. DiCarlo, O. A. Gharbawie, H.-X. Qi, J. H. Kaas, Spinal cord neuron inputs to the cuneate nucleus that partially survive dorsal column lesions: A pathway that could contribute to recovery after spinal cord injury. The Journal of Comparative Neurology 523, 2138–60 (2015).

A. J. Loutit, R. M. Vickery, J. R. Potas, Functional organization and connectivity of the dorsal column nuclei complex reveals a sensorimotor integration and distribution hub. Journal of Comparative Neurology 529, 187–220 (2021).

J. D. Lieber, X. Xia, A. I. Weber, S. J. Bensmaia, The neural code for tactile roughness in the somatosensory nerves. Journal of Neurophysiology 118, 3107–3117 (2017).

A. I. Weber, et al., Spatial and temporal codes mediate the tactile perception of natural textures. Proc. Natl. Acad. Sci. U.S.A. 110, 17107–17112 (2013).

P. R. Douglas, D. G. Ferrington, M. Rowe, Coding of information about tactile stimuli by neurones of the cuneate nucleus. The Journal of Physiology 285, 493–513 (1978).

D. G. Ferrington, S. Horniblow, M. J. Rowe, Temporal patterning in the responses of gracile and cuneate neurones in the cat to cutaneous vibration. The Journal of Physiology 386, 277–291 (1987).

B. D. Gynther, R. M. Vickery, M. J. Rowe, Transmission characteristics for the 1:1 linkage between slowly adapting type II fibers and their cuneate target neurons in cat. Exp Brain Res 105, 67–75 (1995).

R. M. Vickery, B. D. Gynther, M. J. Rowe, Synaptic transmission between single slowly adapting type I fibres and their cuneate target neurones in cat. The Journal of Physiology 474, 379–392 (1994).

B. S. Minnery, R. M. Bruno, D. J. Simons, Response Transformation and Receptive-Field Synthesis in the Lemniscal Trigeminothalamic Circuit. Journal of Neurophysiology 90, 1556–1570 (2003).

K. Sakurai, et al., The Organization of Submodality-Specific Touch Afferent Inputs in the Vibrissa Column. Cell Reports 5, 87–98 (2013).

F. Vega-Bermudez, K. O. Johnson, SA1 and RA Receptive Fields, Response Variability, and Population Responses Mapped with a Probe Array. Journal of Neurophysiology 81, 2701–2710 (1999).

J. D. Lieber, S. J. Bensmaia, Emergence of an Invariant Representation of Texture in Primate Somatosensory Cortex. Cereb Cortex (2020) https:/doi.org/10.1093/cercor/bhz305 (December 26, 2019).

Y.-C. Pei, S. S. Hsiao, J. C. Craig, S. J. Bensmaia, Shape Invariant Coding of Motion Direction in Somatosensory Cortex. PLoS Biology 8, e1000305 (2010).

E. P. Gardner, R. M. Costanzo, Neuronal mechanisms underlying direction sensitivity of somatosensory cortical neurons in awake monkeys. Journal of Neurophysiology 43, 1342–1354 (1980).

B. Babadi, H. Sompolinsky, Sparseness and Expansion in Sensory Representations. Neuron 83, 1213–1226 (2014).

P. M. Daniel, D. Whitteridge, The representation of the visual field on the cerebral cortex in monkeys. The Journal of Physiology 159, 203–221 (1961).

M. A. Biedenbach, Cell density and regional distribution of cell types in the cuneate nucleus of the Rhesus monkey. Brain Research 45, 1–14 (1972).

G. Corniani, H. P. Saal, Tactile innervation densities across the whole body. Journal of Neurophysiology 124, 1229–1240 (2020).

C. Darian-Smith, M. Ciferri, Cuneate nucleus reorganization following cervical dorsal rhizotomy in the macaque monkey: its role in the recovery of manual dexterity. J. Comp. Neurol. 498, 552–565 (2006).

J. Xu, J. T. Wall, Functional organization of tactile inputs from the hand in the cuneate nucleus and its relationship to organization in the somatosensory cortex. Journal of Comparative Neurology 411, 369–389 (1999).

K. C. Catania, D. B. Leitch, D. Gauthier, A Star in the Brainstem Reveals the First Step of Cortical Magnification. PLOS ONE 6, e22406 (2011).

H. Wassle, U. Grunert, J. Rohrenbeck, B. B. Boycott, Retinal ganglion cell density and cortical magnification factor in the primate. Vision Research 30, 1897–1911 (1990).

K. J. Berkley, R. J. Budell, A. Blomqvist, M. Bull, Output systems of the dorsal column nuclei in the cat. Brain Research Reviews 11, 199–225 (1986).

P. Halder, N. Kambi, P. Chand, N. Jain, Altered Expression of Reorganized Inputs as They Ascend From the Cuneate Nucleus to Cortical Area 3b in Monkeys With Long-Term Spinal Cord Injuries. Cerebral Cortex 28, 3922–3938 (2018).

N. Kambi, et al., Large-scale reorganization of the somatosensory cortex following spinal cord injuries is due to brainstem plasticity. Nature Communications 5, 3602 (2014).

C.-C. Liao, J. L. Reed, H.-X. Qi, E. K. Sawyer, J. H. Kaas, Second-order spinal cord pathway contributes to cortical responses after long recoveries from dorsal column injury in squirrel monkeys. Proceedings of the National Academy of Sciences 115, 4258–4263 (2018).

H.-X. Qi, O. A. Gharbawie, K. W. Wynne, J. H. Kaas, Impairment and recovery of hand use after unilateral section of the dorsal columns of the spinal cord in squirrel monkeys. Behavioural Brain Research 252, 363–76 (2013).

M. A. Harvey, Saal, H.P., Dammann, J.F., Bensmaia, S.J., Multiplexing Stimulus Information through Rate and Temporal Codes in Primate Somatosensory Cortex. PLoS Biology 11, e1001558 (2013).

B. Calancie, K. J. Klose, S. Baier, B. A. Green, Isoflurane-induced attenuation of motor evoked potentials caused by electrical motor cortex stimulation during surgery. Journal of Neurosurgery 74, 897–904 (1991).

S. W. Cheung, et al., Auditory cortical neuron response differences under isoflurane versus pentobarbital anesthesia. Hearing Research 156, 115–127 (2001).

T. Noda, H. Takahashi, Anesthetic effects of isoflurane on the tonotopic map and neuronal population activity in the rat auditory cortex. Eur J Neurosci 42, 2298–2311 (2015).

K. K. Sellers, D. V. Bennett, A. Hutt, J. H. Williams, F. Fröhlich, Awake vs. anesthetized: layer-specific sensory processing in visual cortex and functional connectivity between cortical areas. Journal of Neurophysiology 113, 3798–3815 (2015).

V. Shumkova, V. Sitdikova, I. Rechapov, A. Leukhin, M. Minlebaev, Effects of urethane and isoflurane on the sensory evoked response and local blood flow in the early postnatal rat somatosensory cortex. Scientific Reports 11, 9567 (2021).

Alkire Michael T., Hudetz Anthony G., Tononi Giulio, Consciousness and Anesthesia. Science 322, 876–880 (2008).

J.-W. Cheng, A. I. Weber, S. J. Bensmaia, Comparing the effects of isoflurane and pentobarbital on the responses of cutaneous mechanoreceptive afferents. BMC Anesthesiology 13, 10 (2013).

Q. He, et al., Movement gating of cutaneous signals in the cuneate nucleus (2019).

A. K. Suresh, et al., Methodological considerations for a chronic neural interface with the cuneate nucleus of macaques. Journal of Neurophysiology 118, 3271–3281 (2017).

Westling, G., Johansson, R., Vallbo, Å. B. (1976). A method for mechanical stimulation of skin receptors. In Sensory functions of the skin in primates (pp. 151-158). Pergamon.

Y.-C. Pei, et al., A multi-digit tactile motion stimulator. Journal of Neuroscience Methods 226, 80–87 (2014).

O. Schwartz, J. W. Pillow, N. C. Rust, E. P. Simoncelli, Spike-triggered neural characterization. Journal of Vision 6, 13–13 (2006).

Chapter 3 | Suppression of cutaneous responses in the cuneate nucleus of macaques during active movement

3.1 Abstract

To achieve stable and precise movement execution, the sensorimotor system integrates exafferent sensory signals originating from interactions with the external world and reafferent signals caused by our own movements. This barrage of sensory information is regulated such that behaviorally relevant signals are boosted at the expense of irrelevant ones. For example, sensitivity to touch is reduced during movement – when cutaneous signals caused by skin stretch are expected and uninteresting – a phenomenon reflected in a decreased cutaneous responsiveness in thalamus and cortex. Some evidence suggests that movement gating of touch may originate from the cuneate nucleus (CN), the first recipient of signals from tactile nerve fibers along the dorsal columns medial lemniscal pathway. To test this possibility, we intermittently delivered mechanical pulses to the receptive fields (RFs) of identified cutaneous CN neurons as monkeys performed a reach-to-grasp task. As predicted, we found that the cutaneous responses of individual CN neurons were reduced during movement. However, this movement gating of cutaneous signals was observed for CN neurons with RFs on the arm but not those with RFs on the hand. We conclude that sensory gating occurs in the first processing stage along the somatosensory neuraxis and sculpts incoming signals according to their task relevance.

3.2 Introduction

Perhaps more than any other sensory modality, touch occurs during active movements. Indeed, cutaneous signals typically arise in the context of goal-directed interactions with objects

2. This manuscript is under revision.

(Mountcastle, 2005). However, limb movement itself activates tactile nerve fibers – particularly those with receptive fields (RFs) near joints – due to the accompanying skin stretch (Johansson, 1978). As we reach for an object, nerve fibers that innervate the shoulder and elbow become activated (Costanzo & Gardner, 1981). However, the pattern of activation is highly predictable from the movement itself to the point that information about limb posture can be inferred from the patterns of neural activity in these nerve fibers. Given its predictability, it may make sense to suppress this signal to enhance more unpredictable signals such as those arising from object interactions. In fact, noisy, self-generated, or delayed sensory inputs have been shown to disrupt fine motor control and coordinated behavior (Azim & Seki, 2019; Scott, 2016; Shadmehr et al., 2010).

As might be expected, then, sensitivity to cutaneous stimulation has been shown to be reduced during movement (Chapman et al., 1987). Indeed, psychophysical experiments with human observers revealed that cutaneous sensitivity decreases during finger movements (Angel & Malenka, 1982; Bays et al., 2006; Post et al., 1994). The neural correlates for this sensory gating have been observed in local field potentials (or the equivalent) measured in the spinal cord (Confais et al., 2017; Seki & Fetz, 2012), medial lemniscus, thalamus (Chapman et al., 1988), and somatosensory cortex of macaques (Seki & Fetz, 2012) and humans (Kurz et al., 2018). However, the origins of this sensory modulation at the cellular level and its dependence on task and behavioral variables remain to be elucidated.

The cuneate nucleus (CN) is the first stage of processing of tactile signals along the dorsal column medial lemniscal pathway and receives abundant descending inputs from cortex (Conner et al., 2021; Loutit et al., 2020). Accordingly, this tiny structure in the brainstem is well positioned to play a role in task- dependent gain modulation. Recordings of local field potentials in the dorsal column nuclei and medial lemniscus of cats (Aguilar et al., 2003; Ghez & Pisa, 1972) and trigeminal nuclei of mice (Chakrabarti & Schwarz, 2018), and in the CN of monkeys (Chapman et al., 1988) and humans (Insola et al., 2010), have implicated

CN in movement gating. However, this suppression has not been characterized at the single cell level in primates, so many questions remain. For example, it is unclear (1) whether all CN neurons are subject to gating or only a subpopulation is; (2) whether gating is deployed homogeneously over the entire body map or rather sculpts incoming signals depending on their body location; and (3) whether this gating is binary or graded according to movement parameters.

To address these questions, we had Rhesus macaques perform a reach-to-grasp task while we delivered tactile stimuli intermittently to the identified locations of the RFs of cutaneous neurons in CN. As the animals performed the task, we measured neuronal responses, tracked limb movements, and measured the forces exerted by the monkey on the manipulandum. We found that cutaneous responses in CN were systematically suppressed during movement for neurons with receptive fields on the arm but were elevated for neurons with RFs on the palmar surface of the hand, where object contact was anticipated. In some cases, cutaneous responses of arm RF CN neurons were also suppressed during force exertion. Finally, gating was observed for some units before movement initiation and was not observed when the arm was moved passively, demonstrating the top down origins of the observed gating during reach and grasp. We conclude that CN plays a major role in the movement gating of tactile signals.

3.3 Results

We recorded the responses of 31 CN cutaneous neurons from a total of five Rhesus Macaques, which responded to light touch over a restricted patch of skin (Figure 3.1, Figure 3.2). Of these, 18 neurons had RFs on the arm (including one unit on the dorsal surface of the hand), 11 on the palmar surface of hand, and 2 on the back.

Animals were trained to perform a reach-and-grasp task. On each trial, an LED cued the animal to reach to and grasp a joystick-like manipulandum and apply a force the magnitude

of which was also cued by the LED. The animal obtained a water reward if it applied the desired force and held it for the required duration (see Methods for details). After obtaining the reward, the animal returned its arm to the arm rest and the next trial was initiated 2 seconds later. Each trial was then split into different epochs: rest, cue, reach, and grasp. To assess whether CN responses are state dependent, we compared stimulus-evoked responses during rest to those evoked during the other three epochs (Figure 3.1A). To this end, we first aligned the response of each neuron to the onset of each stimulation pulse, computed the response to each stimulation pulse (bottom row of Figure 3.1A), then averaged these separately for each epoch (Figure 3.1B&C). We also computed the mean firing rate (FR) during the inter-pulse intervals to assess how the baseline response varied across epochs (Figure 3.2).

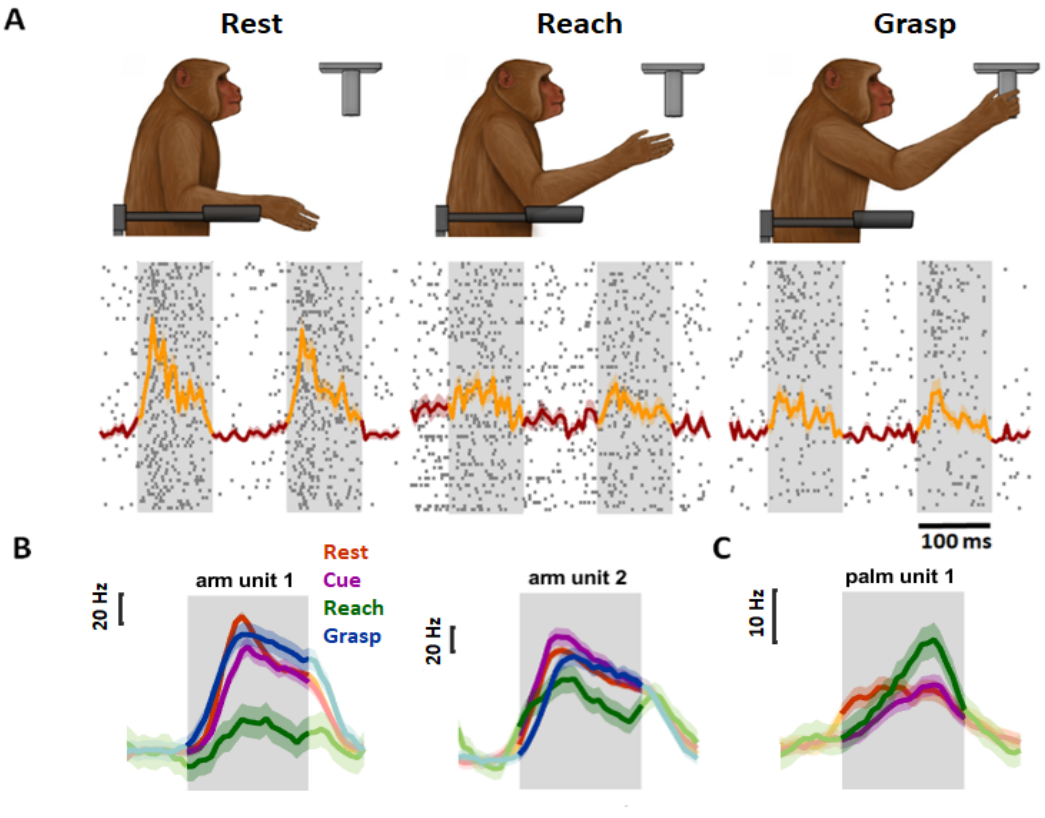

Figure 3.1: Behavioral task and neural data. A| Behavioral task. The monkey placed its free arm onto the arm rest for a varied interval (rest epoch) to initiate a trial cued by an LED. The time between the onset of the LED and the starting of the reaching movement is the cue epoch. The animal then reached toward (reach epoch) and grasped the manipulandum, applied the cued force (force epoch), received a water reward, then returned its arm back to the arm rest and waiting for the start of the next trial. Tactors placed over identified receptive fields pulsed every 200 ms for 100 ms throughout the entire task. One exemplar arm tactile CN neuron's responses over 50 trials are listed below the behavioral diagram. The PSTHs are overlaid on top with orange segments of the PSTH denoting the stimulation-induced response and red segments the baseline. B| Demeaned average responses of two exemplar cutaneous CN arm neurons with RFs on the arm. Gray shading denotes the stimulation epoch. Orange, purple, green, and blue lines stand for the average responses during resting, indication, reaching, and grasping epochs, respectively. C| Same as B but for one exemplar palm unit.

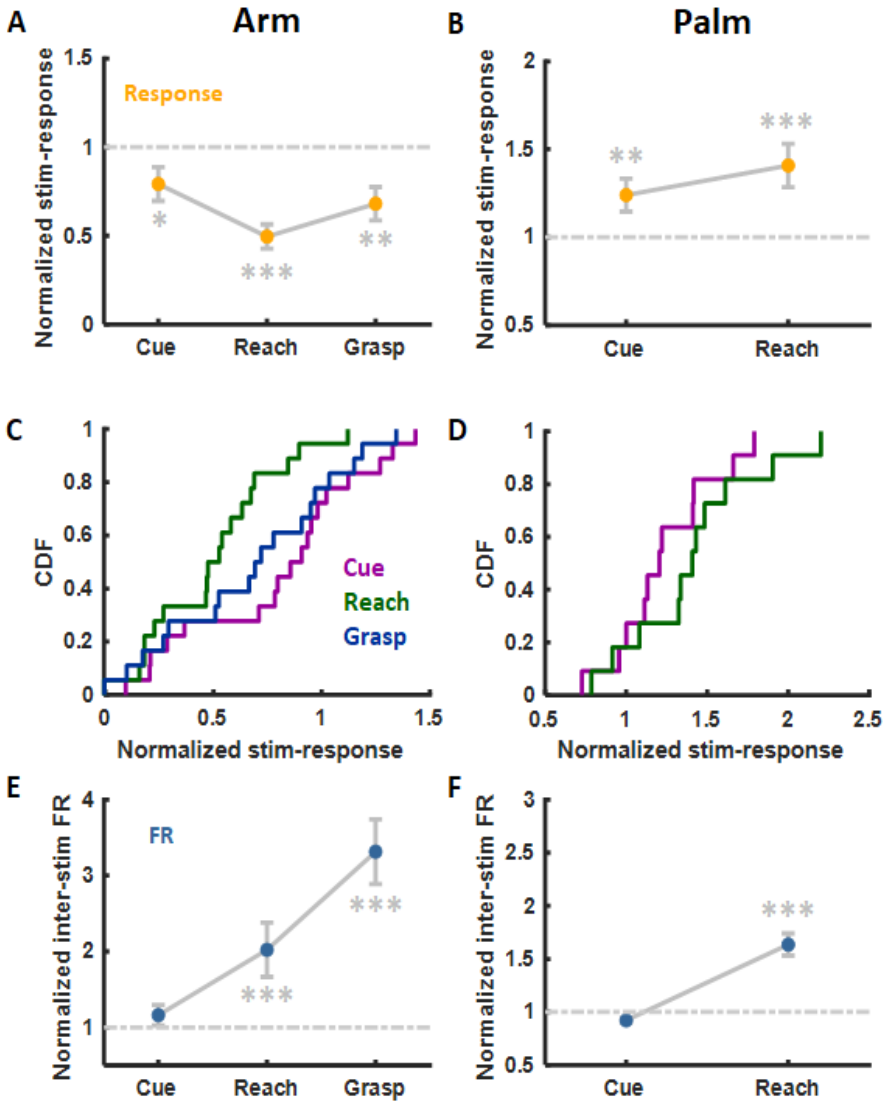

Figure 3.2: Stimulation-evoked and baseline responses of arm and palm cutaneous neurons. A| Mean normalized stimulation-evoked responses of all cutaneous neurons with RFs on the arm (n=18) to stimulation during four event epochs normalized to the rest responses. Responses were significantly reduced during the cue, the movement and the force epochs. B| Mean stimulation-evoked responses of all cutaneous neurons with RFs on the palmar surface of the hand (n=11) during different event epochs. Responses were significantly increased during the movement epochs. C| Cumulative histograms of normalized stim-responses of all arm neurons during the three behavioral epochs. D| The same thing as in C but for all palm neurons. E| Mean baseline response to the same arm neurons as in A. Baseline firing rates were significantly elevated during grasp compared to rest. F— Mean baseline responses of the same palm units as in B. (*p<0.05, **p<0.01, ***p<0.001, significant deviation from rest epoch, Wilcoxon signed-rank test).

3.3.1 Behaviorally dependent modulation of cutaneous responses

To gauge the response modulation, we divided the mean stimulus-evoked response during each epoch by the mean stimulus-evoked response during rest. Accordingly, values greater than 1 indicated elevated responses with respect to rest whereas values less than 1 indicated suppression. We expected the stimulation-evoked response of arm cutaneous neurons to be weaker during the movement epochs and perhaps during the force generation epochs compared to their rest counterparts. As predicted, the tactile responses of arm cutaneous units were significantly weaker during movement and force generation epochs (Figure 3.2A), as evidenced by normalized stim-responses below 1 during movement. The attenuation of the responses occurred even before the start of movement, as shown by the decreased responses during the cue epoch. Note that the baseline response during the cue and rest epochs were equivalent, confirming that the observed gating during the former was not movement-related. The presence of such gating during preparation phase implicates descending inputs.

Note, however, that the baseline responses – measured during the inter-pulse intervals – were elevated during the movement and force generation epochs (Figure 3.2E), opening up the possibility that the reduced activity during movement and force epochs reflected saturation of the responses when reafferent and exafferent signals co-occur. Several lines of evidence rule out the possibility that saturation caused the observed suppression. First, there was no relationship between the strength of the movement gating and the baseline (non-stimulus evoked) activity (Figure 3.2). That is, neurons whose response increased the most during movement or those whose baseline firing rate was highest did not systematically exhibit the strongest suppression during movement. Hence, movement induced gating is not a trivial consequence of response saturation.

3.3.2 Dependence of the gain modulation on behavioral variables

The suppression of cutaneous sensitivity at the lemniscal, thalamic, and cortical levels has been shown to be dependent on the speed of movement (Chapman et al., 1988; Ghez & Pisa, 1972). With this in mind, we examined the degree to which the suppression was modulated by behavioral parameters, including movement speed as well as applied force. We found that, of the 18 cutaneous neurons with RFs on the arm, two showed significantly stronger gating at higher speeds during the movement epoch (Figure 3.1A). The influence of grasp force on modulation (during the grasp epoch) are more varied: Three neurons showed significantly elevated and two showed significantly suppressed responses at higher grasp forces (Supplementary Figure 3.1B). Thus, the dependence of the gain modulation on behavioral variables is heterogeneous: The gating is all-or-none of some neurons and graded according to behavior in others.

3.3.3 Movement gating on the hand and back

All the analyses described above were performed on cutaneous neurons with RFs on the arm. A handful of recorded neurons had cutaneous RFs on the glabrous skin (palmar surface) of the hand. Unlike their counterparts with receptive fields on the arm, all CN neurons with RFs on the glabrous skin exhibited elevated stimulus-evoked responses during the movement epoch (Figure 3.2 B&D). Responses of hand neurons during grasping epochs were not included for analysis because contact with the manipulandum would contaminate stimulus-evoked responses. Two other units had receptive fields on the back and were not significantly modulated during movement (Figure 3.3; Supplementary Figure 3.4), further indicating that the state dependent effects observed was not due to trivial side effects of stimulators. The modulation of cutaneous sensitivity thus seems to depend on RF location, which may reflect the task relevance of signals from different body regions: Signals from the proximal limb reflect reafferences and are not particularly informative whereas signals from

the hand carry information about contact with the manipulandum and are thus critical to task performance.

3.3.4 Movement gating during imposed movement

To assess the degree to which the observed task-related modulation of cutaneous sensitivity was mediated by top-down signals, we compared the stimulus-evoked responses during active movements and passively imposed movements. To the extent that gating was caused by top-down signals, we expected it to be absent in the passive condition. We found that, indeed, the stimulus-evoked responses of CN neurons with RFs on the arm were not significantly different during imposed arm movements than during rest (Figure 3.3A; $p = 0.8041$, Wilcoxon rank sum test) and were significantly elevated compared to those measured during active reach ($p < 0.001$). Similarly, the responses of CN neurons with RFs on the glabrous skin were not significantly modulated during passively imposed movements ($p = 0.9345$) and were significantly lower compared to those measured during active reach (Figure 3.3B; $p < 0.001$). That movement gating of sensory signals is only observed during actively generated movements is consistent with the hypothesis that this gating originates centrally.

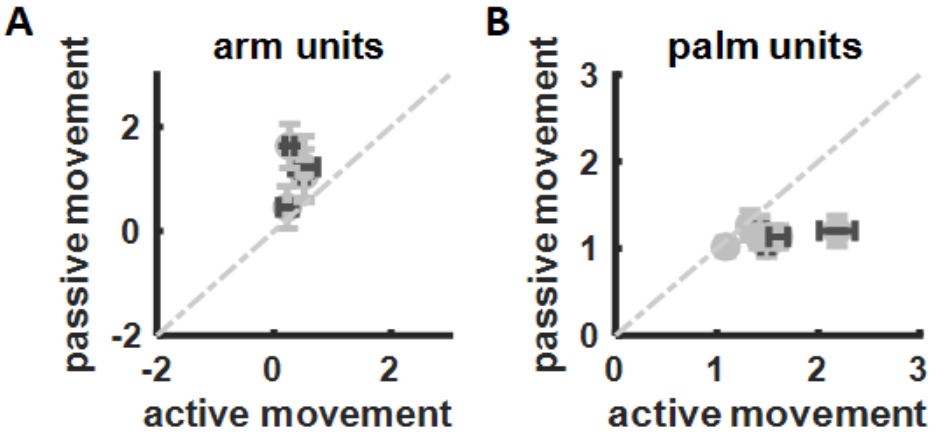

Figure 3.3: Stimulation-evoked responses of arm and palmar cutaneous neurons under active vs. passive movement. A| Mean stimulation-evoked responses of all cutaneous neurons with RFs on the arm (n=4) to stimulation during three event epochs normalized to the rest responses. A darker color error bar on the abscissa or ordinate denotes a significant movement-related modulation under active or passive conditions, respectively. None of the four units showed significantly reduced responses during passive manipulations. B| Mean stimulation-evoked responses of all cutaneous neurons with RFs on the palm (n=6). None of the six units showed significantly elevated responses during passive manipulations. (Wilcoxon rank sum test).

3.4 Discussion

In summary, we show that the cutaneous sensitivity of CN neurons with RFs on the proximal limb is systematically suppressed during reaching movements. In contrast, the sensitivity of CN neurons with RFs on the hand is either unaffected or elevated. In some neurons, cutaneous sensitivity is also modulated as the animal applies isometric forces on the manipulandum, in the absence of movement. The modulation of CN responses has a central origin as evidenced by the fact that it is observed even before movement – i.e., before exafference is engaged – and only during active reaching movements. The strength of the modulation varies across neurons from 5 to 95% suppression for the arm and from 20% to 250% elevation for the hand. The dependence of modulation on behavioral parameters – including movement speed or exerted force – also varies widely across neurons: In most neurons the

modulation is all-or-none whereas, in a subpopulation, the modulation is graded by the speed or exerted force. Our results are consistent with the view that top-down signals sculpt the sensory input to squelch behaviorally irrelevant and possibly distracting cutaneous signals and enhance behaviorally relevant signals.

3.4.1 Sculpting of cutaneous signals according to task relevance

We show that cutaneous sensitivity is not homogeneously gated over the entire body during a reaching movement. CN neurons with RFs on the arm are suppressed, CN neurons with RFs on the glabrous skin are sensitized, and CN neurons with RFs on the back are unaffected. This spatial specificity of gating has also been observed on humans as modulation decreased when one proceeded away from the moving segment (Post et al., 1994; Williams et al., 1998). Furthermore, the selective inhibition shown in the present study mirrors results from psychophysical experiments which observed that the detection threshold at the forearm increased while those of distal digits did not during reach-and-grasp task (Colino et al., 2014). The differential modulation of signals from different body regions may reflect their differential utility in accomplishing a task (Juravle et al., 2017). In a reach-to-grasp task, cutaneous signals from the palmar surface of the hand signal contact with the manipulandum and trigger the end of the grasp (Johansson & Flanagan, 2009), whereas signals from the arm reflect reafference and are less behaviorally relevant. The observed modulation would then enhance the task-relevant hand signals and suppress the task-irrelevant arm signals. A similar phenomenon was observed in a psychophysical study with humans, which showed that detection thresholds increased on the forearm but not the hand during a reach-to-grasp task (Colino et al., 2014). The task-dependence of modulation has been observed in a variety of contexts, not limited to upper limb behavior (Juravle et al., 2013; Staines et al., 2000, 2002).

3.4.2 Dependence of modulation on behavioral variables

We find that the magnitude of the modulation is largely independent of behavioral variables, such as movement speed and applied force. Indeed, only a few CN neurons exhibited cutaneous responses whose strength depended on the speed of the reach or the force applied on the manipulandum. For most neurons, the modulation was all-or-none. These findings at the single-cell level are broadly consistent with the observation that lemniscal potentials measured in cats and primates are more suppressed at higher velocities (Chapman et al., 1988; Ghez & Pisa, 1972; Rushton et al., 1981). Indeed, field potentials reflect the mixed activity of neurons that exhibit speed-dependent and speed-independent suppression. Similarly, sensory thresholds measured in human observers have been shown to increase with movement speed (Angel & Malenka, 1982; Schmidt et al., 1990). These results stand in contrast to the all-or-none gating in the trigeminal nucleus and barrel cortex of rats (Chakrabarti & Schwarz, 2018; Hentschke et al., 2006).

Studies of the effect of force exertion on cutaneous sensitivity have yielded mixed results. Varying isometric force was found to have no effect on cutaneous signals measured in the somatosensory cortex of humans (Rushton et al., 1981) or on medial lemniscus potentials in cats (Ghez & Pisa, 1972). However, forces exerted by the lower limb did modulate cutaneous signals in cortex in a graded fashion (Cohen & Starr, 1985; Sakamoto et al., 2004; Wasaka et al., 2005). In line with the latter result, psychophysical experiments with human observers revealed an increase in detection thresholds during higher isometric force production (Post et al., 1994). This seeming heterogeneity across studies may reflect the fact that only a small subpopulation of CN neurons exhibits a force-dependent modulation so these effects may be subtle at the population level and dependent on the specific ranges of forces applied and on the spatial relationship between activated muscles and locus of cutaneous stimulation.

3.4.3 Central origins of modulation

The modulation of tactile sensitivity observed in the present study likely has a central origin. Indeed, cutaneous responses are suppressed or enhanced before movement onset and this modulation is not observed during passive movements. A putative circuit to mediate this centrally driven modulation has been identified in rodents. Indeed, the core region of the rodent CN receives the bulk of the input from the periphery whereas the outer shell comprises mostly inhibitory interneurons (Conner et al., 2021). The core region receives excitatory inputs from somatosensory cortex whereas the shell receives both excitatory and inhibitory input from a variety of motor structures. Together, these top down pathways can account for the observed modulation of cutaneous sensitivity. Excitatory projections from motor cortex to inhibitory neurons in the shell region could account for the suppression of cutaneous signals. Excitatory projections from somatosensory cortex to the core region or inhibitory projections from motor cortex to the shell region account for the observed elevation of cutaneous sensitivity. While the relevant anatomy of rodents and primates differs, similar principles likely underlie the present findings. Indeed, primate CN also receives a mix of excitatory and inhibitory inputs from cortex (Biedenbach, 1972; Loutit et al., 2020).

3.4.4 Modulation in other sensory modalities

Visual signals are processed via multiple synapses in the retina, but this early processing as it is not subject to top-down influences. The first opportunity for the central modulation of visual input is in the lateral geniculate nucleus, which indeed receives massive feedback projections from visual cortex (Reppas et al., 2002; Sillito et al., 1994). Similarly, auditory signals are not subject to central modulation at stages of processing before the medial geniculate nucleus, which again receives significant projections from downstream structures (Reznik et al., 2015; Schneider et al., 2014, 2018). That top-down modulation occurs at the very first synapse for touch may be a unique feature of the dorsal column medial lemnisical

pathway. Note, however, that top down projections to the outer hair cells shape auditory afferent signals (Wersinger & Fuchs, 2011) and may play a similar function as does the direct modulation of sensory afference described here for touch.

3.5 Methods

3.5.1 Experimental apparatus

A joystick was mounted to a high-sensitivity force sensor (ATI Six-Axis Force/Torque Transducer). Two arrays of LEDs were placed on top of force sensor with one array of it cueing the grasp force that the monkey needs to exert to obtain a reward and another reflecting the real-time loads the monkey applied. Tactile stimulation was delivered using DC coreless vibration motors (7mm $\times$ 25mm, Speed: 8000-24000RPM, Tatoko), which were fixed to various locations on the monkeys' arms, each corresponding to one identified cutaneous RF of a CN neuron. The onset of movement was signaled by photoresistors embedded in the arm rest of the monkey chair and arm and hand movements were tracked using a camera and two wireless motion trackers attached to the upper and lower arm (Xsens 3D Motion Tracking System, Enschede, Netherlands).

3.5.2 Behavioral paradigm

We trained five rhesus macaques (four males, one female, ages 5-10 yr) to perform a reach-and-grasp task (Figure 3.1A). Monkeys were seated upright at the experimental chair, with one arm restrained and the other free, facing LEDs and the joystick (Figure 3.1B). The animal placed its free arm onto the arm rest for a random delay of 0.5-2s (rest epoch) to initiate a trial. A trial began when the first row of LED lit up, signaling the monkey to initiate a reach towards the manipulandum. The LED prescribed the amount of force, which varied across trials, that the monkey needed to apply to the manipulandum on that trial.

Application of a sustained load on the joystick activated the second row of LEDs, with the number of lights proportional to the applied force. If the amount of force the monkey exerted exceeded the required force and the monkey held the force for a required interval (varying between 0.1-2.0s; hold), the monkey would receive a liquid reward. The animal then returned to the arm rest for 2s, received the second water reward, the LEDs turned off, and the animal waited for the initiation of the next trial. Recordings from the first reward onset to the end of every trial were not included in data analysis to minimize the influence of task-unrelated movement, as these intervals were accompanied by reward intakes.

Before the start of every recording session, we performed receptive field mapping to locate tactile CN units. We classified a unit as cutaneous if it responded to gentle stroking of the skin but not to lengthening and palpation of the muscle underneath the skin. During recording sessions, 60-100Hz vibrations were applied to the receptive fields of identified CN units in regular intervals (100ms stimulus on, 100ms stimulus off). The vibrating tactors were firmly attached to the pre-shaved receptive fields of investigated neurons using glue and then three layers of vet wrap were applied around the tactor. As the animal performed the task, arm movements were tracked using two accelerometers attached proximal and distal arms via velcro bands. Data recorded from days where clear displacement of tactors or accelerometers were observed at the end of recording sessions were excluded. A camera was placed in front of the monkey and was checked at the beginning of every experimental session to ensure a view that includes the whole behavioral process. All camera recordings were manually checked and trials during which monkeys exhibited clear task-unrelated movement fluctuations were excluded. A publicly available motion-tracking package was used to track monkey's arm movement and to infer reaching speeds based on videos (DeepLabCut, Mathis et al., 2018). On some trials, we manually manipulated monkey's hand to passively perform the reach and grasp task. For this task, we followed the same procedure as the active reaching task (Figure 1), except that the experimenter held the monkey's arm to reach and grasp the manipuladum

and return to arm-rest. Experimenter's contact with tactor placed on monkey's RFs was avoided during passive trials. Post-hoc analysis and reexaminations of recorded videos were done to exclude passive trials with clear voluntary movement of the monkeys. We used Wilcoxon rank sum test to examine the evoked responses of the same set of neurons under active and passive movement conditions.

3.5.3 Neural Data Acquisition

We implanted 96-channel iridium-oxide Utah arrays (UEA) (Blackrock Microsystems, Inc., Salt Lake City, UT) in all five monkeys. We used customized 8x12 shank rectangular array with 1.5 mm electrode length and 9cm wire bundle length between array and pedestal to maximize the landing on CN. Neural data were acquired using a digital CerePlex E headstage and CerePlex Direct acquisition system (Blackrock Microsystems). We bandpass-filtered neural signals between 250 Hz and 5000 Hz and we set the voltage threshold for every channel manually before the start of every recording session. We recorded time of every threshold crossing on every channel and saved neural waveform in 1.6 ms window for off-line spike sorting (Plexon, Dallas, TX).

We simultaneously recorded timestamps that indicated when stimulation and behavioral events occurred, along with the neural data while the monkey performed the task.

3.5.4 Surgical Procedures

All experimental protocols were reviewed and approved by the University of Chicago Animal Care and Use Committee and complied with the National Institutes of Health Guide for the Care and Use of Laboratory Animals. We anesthetized animal using ketamine HCI (3 mg/kg im) and dexmedetomidine (75 µg/kg) and fixed animal's head in a stereotaxic frame such that neck was flexed to be 75 degree relative to the body to allow for maximum exposure of brainstem. We first made a midline incision from the occipital bone to approximately

C1 C3 and removed posterior cervical muscles along midline using cautery. We secured the pedestal to the skull with bone screws on the other hemisphere as opposed to the array implantation side such that the routing of the array lead between it and the array in the brainstem will be flexible enough for the monkey to make normal neck movement. Then we exposed the foramen magnum and the occipitocervical dura using cautery and sharp dissection. We identified the location of Obex and used the stereotaxic frame to target 2mm lateral to midline and 2 mm anterior to Obex to aim for maximum coverage of distal limb cutaneous regions of upper body (Darian-Smith Ciferri, 2006; Loutit et al., 2020; Qi Kaas, 2006; Suresh et al., 2017; Versteeg et al., 2021). Then UEA was implanted into the brainstem using the pneumatic inserter (BlackRock microsystem).

3.5.5 Data Analysis

Offline Redefinition of Task Epochs

To evaluate the epoch-dependent modulation of FR and responses, we first defined each behavioral epoch by analyzing photoresistors, accelerometers and force input. Reaching onset was defined as the first time when photoresistors on the arm rest were uncovered (start reaching) while reaching epoch offset was defined as the first time that force applied on manipulandum rose above the threshold (start holding). Both start and end of reaching behavior were confirmed with rapid and steady decreases in the acceleration of the arm.

After finding the onset and offset points of reaching, we defined four movement-related epochs for analysis: (1) rest, from the start of the photoresistors coverage till the onset of the cue signal; (2) delay/cue, from onset of cue signal to onset of volitional movement judged from accelerometer recordings; (3) reach, from onset of photoresistors uncovering time to onset of grasping with force exerted crossing force threshold; (4) grasp, from onset of joy-stick contact to start of water reward after monkey achieved required grasping force (Figure 3.1A). Only the trials during in which all behavioral events were properly recorded, were analyzed. In

addition, to minimize the possibility of movements during resting and cue epoch, we only included stimulation snippets surrounded by baseline FRs that are within three standard deviations away from the mean FR during these two epochs.

Compiling Stimulation-Elicited Response and Firing Rates for Each Behavioral Epoch

For each RF-stimulated and recorded neuron, the stim-elicited response was computed by pooling the stim-on firing rates over the whole 100 ms stimulation phases recorded during the task so as to maximize the signal-to-noise ratio, minus the mean 100 ms stim-off FR. We first generated a PSTH, aligned to onset of all stimulation pulses applied during the task, and then we took the averages of all stim-on and stim-off intervals. The average PSTH included the data from 50 ms before to 50 ms after the 100ms stimulation pulse, with a bin size of 5ms. Then we computed the average 100ms stim-on FR and subtracted the average 50ms pre-stimulation inter-stimulus FR from it to obtain the demeaned stimulus-elicited response of every neuron during that specific event epoch (Figure 3.1Bc). We also calculated the inter-stimulus firing (FR) of every event epoch, defined as the average 100ms stim-off FR of each epoch, to reflect the baseline status of every neuron during that epoch.

For every neuron, normalization was achieved by dividing the stim-evoked responses/inter-stim FR in each event epoch by the mean resting state stim-responses/inter-stim FR of that neuron (Figure 3.2). (In sum, all 'response' talked about in this paper refer to stimulation-elicited response to differentiate from 'FR', which refers to inter-stimulus firing rate.) We compared the rest-epoch average response/FR with those of the other three epochs (cue, reach, and grasp) using Wilcoxon signed-rank test to study the modulation effect during active portions of the task.

Dependence of Gating on Movement Speed

To investigate the influence of movement speed on the degree of gating, we first derived reaching and speed of every trial using DeepLabCut. We manually labeled 50 videos randomly sampled from all monkeys to train DeepLabCut and then generated the reaching and return speed of all trials. All speed during resting period was spitted into four quartiles and the mean normalized stim-responses of these four quartiles were plotted against speed quartiles for every neuron (Supplementary Figure 3.1).

For every neuron, normalization was achieved by dividing the stim-evoked responses/inter-stim FR in each event epoch by the mean resting state stim-responses/inter-stim FR of that neuron (Figure 3.2). (In sum, all 'response' talked about in this paper refer to stimulation-elicited response to differentiate from 'FR', which refers to inter-stimulus firing rate.) We compared the rest-epoch average response/FR with those of the other three epochs (cue, reach, and grasp) using Wilcoxon signed-rank test to study the modulation effect during active portions of the task.

Dependence of Gating on Force parameters

To study the influence of load of modulation, we combined data from grasping epochs of all cutaneous units on the arm across all experimental sessions. We categorized the whole grasping force range into low (lowest 1/2) and high conditions (strongest 1/2). We then averaged the stim-elicited responses of the two grasping levels and studied the effects of laods on gating using Wilcoxon signed-rank test (Supplementary Figure 3.1).

Influence of the Firing Rate Saturation Effects on Movement Gating

Although the decrease in response during movement and force epochs could be evidence of the state-dependence of CN tactile neurons, it could also be due to the high firing rates and

thus decreased room for increase in excitability during nonstationary states. To rule out the possibility of this saturation effect, we calculated baseline resting stage inter-stim firing rates as an index of the excitability. We then examined the influence of baseline excitability of each neuron on its own responses by relating baseline firing rates to amount of suppression, namely the difference in stim-elicited responses in movement and no movement conditions (Figure 3.2).

3.5.6 Supplementary Figures

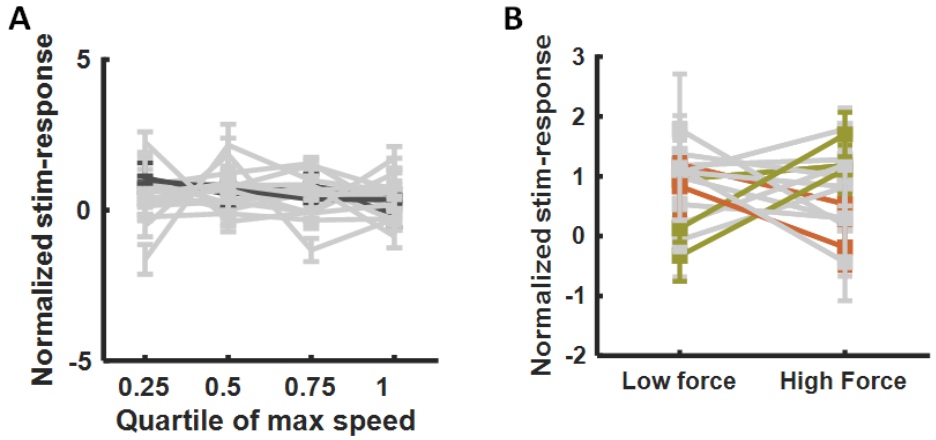

Supplementary Figure 3.1: Modulation effect dependency on movement parameters. A| Diagram shows the effects of different reaching speeds on normalized stimulus evoked responses, which is the ratio of the stimulus evoked responses during movement to its counterparts during rest, as shown in figure B. Every line stands for one cutaneous arm neuron and neurons that were significantly influenced by movement speed were plot in darker grey while the others in lighter grey. B| Diagram shows the degrees of grasping force on normalized stimulus evoked responses. Every line stands for one cutaneous arm neuron and neurons that showed significantly more elevated responses as force increases were plotted in green, significantly more inhibited responses as force increases would be plotted in red, and the rest in light grey.

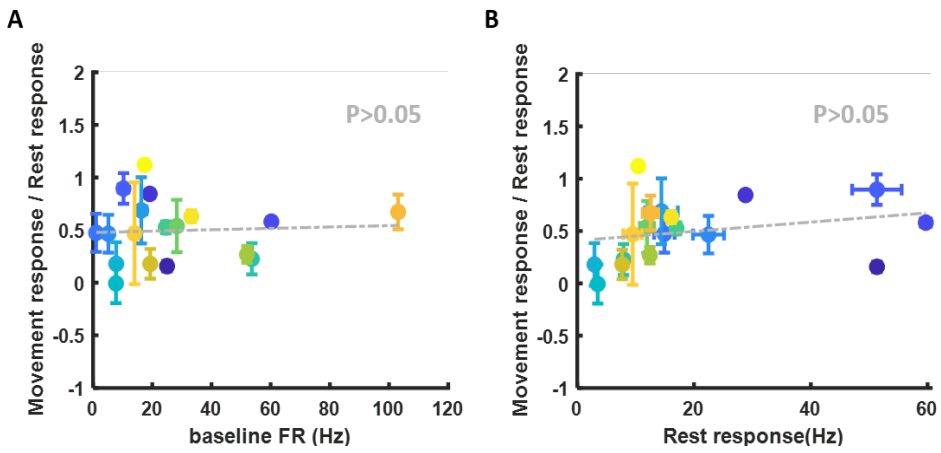

Supplementary Figure 3.2: Saturation effects analysis. A| The effects of baseline firing rates on the degree of normalized stim-evoked responses during movement. Colors correspond to different neurons. Dotted line denote the fitted line, the slope of which is not significantly different from 0. B| The same thing as A but plotted against stim-elicited responses during rest. The data do not show a saturation effect.

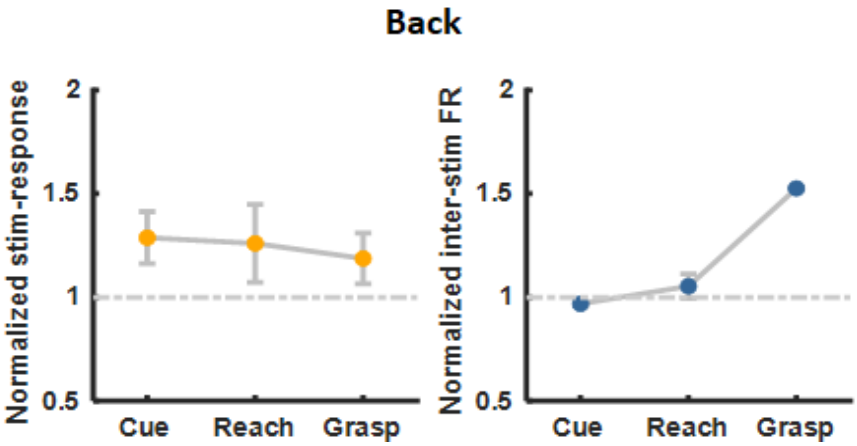

Supplementary Figure 3.3: Stimulus-evoked response and firing rates modulation of back cutaneous neurons. A| The same stimulus-elicited response plot as fig. 2A but for all tactile neurons with RFs on the back (n=2). B| The same inter-stimulus firing rate plot as fig. 2B but for back cutaneous units. No significant changes were observed during any event epoch for both stim-evoked response and firing rates. (*p<0.05, **p<0.01, ***p<0.001, significant deviation from rest epoch, Wilcoxon signed-rank test).

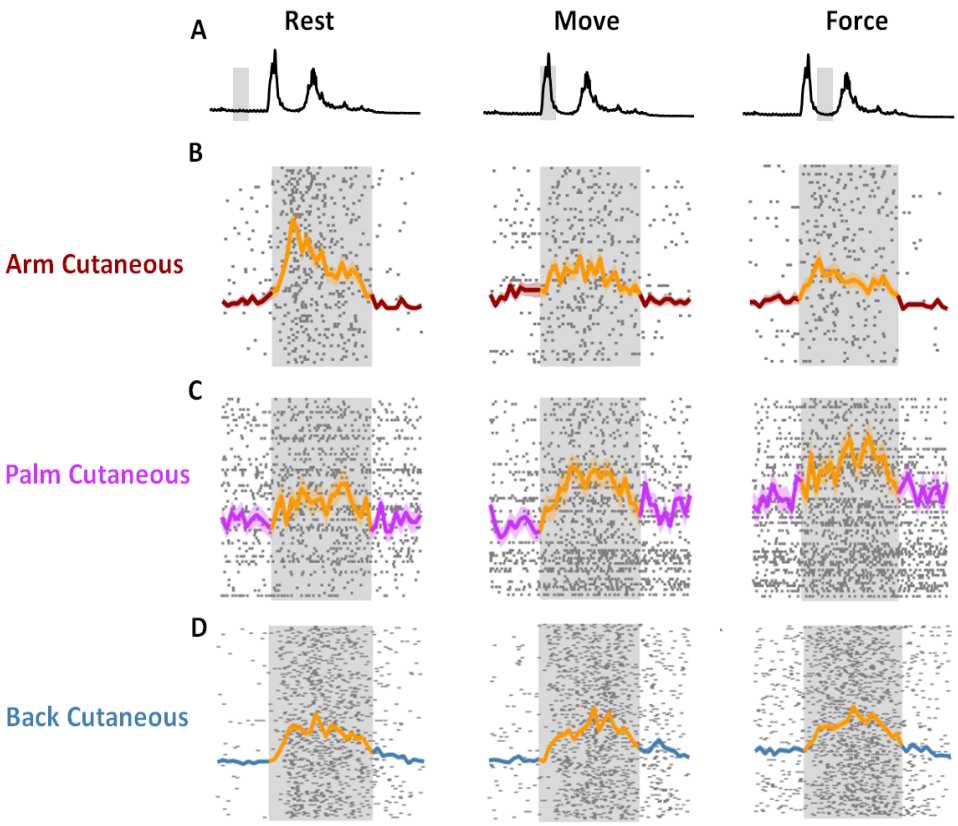

Supplementary Figure 3.4: Exemplar stim-elicited responses of different classes of neurons. A| Average acceleration traces with grey backgrounds highlighting the event epoch. B| Three exemplar segments of responses of arm cutaneous neuron during rest, move, and force epochs. Every row stands for neural responses of one trial. Grey back ground stands for 100ms stimulation interval while white back grounds stand for 100ms inter-stimulus interval. Overlaid curves are PSTH. C| Same as B but from a palmar surface cutaneous units. D| Same as B but from a back cutaneous unit.

3.6 References

Aguilar, J., Rivadulla, C., Soto, C., & Canedo, A. (2003). New Corticocuneate Cellular Mechanisms Underlying the Modulation of Cutaneous Ascending Transmission in Anesthetized Cats. Journal of Neurophysiology, 89(6), 3328–3339.

Angel, R. W., & Malenka, R. C. (1982). Velocity-dependent suppression of cutaneous sensitivity during movement. Experimental Neurology, 77(2), 266–274.

Azim, E., & Seki, K. (2019). Gain control in the sensorimotor system. Current Opinion in

Physiology, 8, 177–187.

Bays, P. M., Flanagan, J. R., & Wolpert, D. M. (2006). Attenuation of Self-Generated Tactile Sensations Is Predictive, not Postdictive. PLoS Biology, 4(2), e28.

Biedenbach, M. A. (1972). Cell density and regional distribution of cell types in the cuneate nucleus of the Rhesus monkey. Brain Research, 45(1), 1–14.

Chakrabarti, S., & Schwarz, C. (2018). Cortical modulation of sensory flow during active touch in the rat whisker system. Nature Communications, 9(1), 3907.

Chapman, C. E., Jiang, W., & Lamarre, Y. (1988). Modulation of lemniscal input during conditioned arm movements in the monkey. Experimental Brain Research, 72(2).

Cohen, L. G., & Starr, A. (1985). Vibration and muscle contraction affect somatosensory evoked potentials. Neurology, 35(5), 691–691.

Colino, F. L., Buckingham, G., Cheng, D. T., van Donkelaar, P., & Binsted, G. (2014). Tactile gating in a reaching and grasping task. Physiological Reports, 2(3), e00267.

Confais, J., Kim, G., Tomatsu, S., Takei, T., & Seki, K. (2017). Nerve-Specific Input Modulation to Spinal Neurons during a Motor Task in the Monkey. The Journal of Neuroscience, 37(10), 2612–2626.

Conner, J. M., Bohannon, A., Igarashi, M., Taniguchi, J., Baltar, N., & Azim, E. (2021). Modulation of tactile feedback for the execution of dexterous movement [Preprint]. Neuroscience.

Costanzo, R. M., & Gardner, E. P. (1981). Multiple-joint neurons in somatosensory cortex of awake monkeys. Brain Research, 214(2), 321–333.

Darian-Smith, C., & Ciferri, M. (2006). Cuneate nucleus reorganization following cervical dorsal rhizotomy in the macaque monkey: Its role in the recovery of manual dexterity. The Journal of Comparative Neurology, 498(4), 552–565.

Ghez, C., & Pisa, M. (1972). Inhibition of afferent transmission in cuneate nucleus during voluntary movement in the cat. In Brain Research (Vol. 40, Issue 1, pp. 145–151).

Hentschke, H., Haiss, F., & Schwarz, C. (2006). Central Signals Rapidly Switch Tactile Processing in Rat Barrel Cortex during Whisker Movements. Cerebral Cortex, 16(8), 1142–1156.

Insola, A., Padua, L., Mazzone, P., & Valeriani, M. (2010). Effect of movement on SEPs generated by dorsal column nuclei. Clinical Neurophysiology, 121(6), 921–929.

Johansson, R. S. (1978). Tactile sensibility in the human hand: Receptive field characteristics of mechanoreceptive units in the glabrous skin area. The Journal of Physiology, 281(1), 101–125.

Johansson, R. S., & Flanagan, J. R. (2009). Coding and use of tactile signals from the fingertips in object manipulation tasks. Nature Reviews. Neuroscience, 10(5), 345–359.

Juravle, G., Binsted, G., & Spence, C. (2017). Tactile suppression in goal-directed movement. Psychonomic Bulletin & Review, 24(4), 1060–1076.

Juravle, G., McGlone, F., & Spence, C. (2013). Context-dependent changes in tactile perception during movement execution. Frontiers in Psychology, 4.

Kurz, M. J., Wiesman, A. I., Coolidge, N. M., & Wilson, T. W. (2018). Haptic exploration attenuates and alters somatosensory cortical oscillations. Journal of Physiology, 596(20), 5051–5061.

Loutit, A. J., Vickery, R. M., & Potas, J. R. (2021). Functional organization and connectivity of the dorsal column nuclei complex reveals a sensorimotor integration and distribution hub. Journal of Comparative Neurology, 529(1), 187-220.

Mathis, A., Mamidanna, P., Cury, K. M., Abe, T., Murthy, V. N., Mathis, M. W., & Bethge, M. (2018). DeepLabCut: Markerless pose estimation of user-defined body parts with deep learning. Nature Neuroscience, 21(9), 1281–1289.

Mountcastle, V. B. (2005). The Sensory Hand: Neural Mechanisms of Somatic Sensation. Harvard University Press. Post, L. J., Zompa, I. C., & Chapman, C. E. (1994). Perception of vibrotactile stimuli during motor activity in human subjects. Experimental Brain Research, 100(1).

Qi, H.-X., & Kaas, J. H. (2006). Organization of primary afferent projections to the gracile nucleus of the dorsal column system of primates. The Journal of Comparative Neurology, 499(2), 183–217.

Reppas, J. B., Usrey, W. M., & Reid, R. C. (2002). Saccadic Eye Movements Modulate Visual Responses in the Lateral Geniculate Nucleus. Neuron, 35(5), 961–974.

Reznik, D., Ossmy, O., & Mukamel, R. (2015). Enhanced Auditory Evoked Activity to Self-Generated Sounds Is Mediated by Primary and Supplementary Motor Cortices. Journal of Neuroscience, 35(5), 2173–2180.

Rushton, D. N., Roghwell, J. C., & Craggs, M. D. (1981). Gating of somatosensory evoked potentials during different kinds of movement in man. Brain, 104(3), 465-491.

Sakamoto, M., Nakajima, T., Wasaka, T., Kida, T., Nakata, H., Endoh, T., Nishihira, Y., & Komiyama, T. (2004). Load- and cadence-dependent modulation of somatosensory evoked potentials and Soleus H-reflexes during active leg pedaling in humans. Brain Research, 1029(2), 272–285.

Schmidt, R. F., Schady, W. J. L., & Torebjörk, H. E. (1990). Gating of tactile input from the hand. Experimental brain research, 79(1), 97-102.

Schneider, D. M., Nelson, A., & Mooney, R. (2014). A synaptic and circuit basis for corollary discharge in the auditory cortex. Nature, 513(7517), 189–194.

Schneider, D. M., Sundararajan, J., & Mooney, R. (2018). A cortical filter that learns to suppress the acoustic consequences of movement. Nature, 561(7723), 391–395.

Scott, S. H. (2016). A Functional Taxonomy of Bottom-Up Sensory Feedback Processing for Motor Actions. Trends in Neurosciences, 39(8), 512–526.

Seki, K., & Fetz, E. E. (2012). Gating of Sensory Input at Spinal and Cortical Levels during Preparation and Execution of Voluntary Movement. Journal of Neuroscience, 32(3), 890–902.

Shadmehr, R., Smith, M. A., & Krakauer, J. W. (2010). Error Correction, Sensory Predic-

tion, and Adaptation in Motor Control. Annual Review of Neuroscience, 33(1), 89–108.

Sillito, A. M., Jones, H. E., Gerstein, G. L., & West, D. C. (1994). Feature-linked synchronization of thalamic relay cell firing induced by feedback from the visual cortex. Nature, 369(6480), 479–482.

Staines, W. R., Brooke, J. D., & McIlroy, W. E. (2000). Task-relevant selective modulation of somatosensory afferent paths from the lower limb: NeuroReport, 11(8), 1713–1719.

Staines, W. R., Graham, S. J., Black, S. E., & McIlroy, W. E. (2002). Task-Relevant Modulation of Contralateral and Ipsilateral Primary Somatosensory Cortex and the Role of a Prefrontal-Cortical Sensory Gating System. NeuroImage, 15(1), 190–199.

Suresh, A. K., Winberry, J. E., Versteeg, C., Chowdhury, R., Tomlinson, T., Rosenow, J. M., Miller, L. E., & Bensmaia, S. J. (2017). Methodological considerations for a chronic neural interface with the cuneate nucleus of macaques. Journal of Neurophysiology, 118(6), 3271–3281.

Versteeg, C., Rosenow, J. M., Bensmaia, S. J., & Miller, L. E. (2021). Encoding of limb state by single neurons in the cuneate nucleus of awake monkeys. Journal of Neurophysiology, 126(2), 693–706.

Wasaka, T., Nakata, H., Kida, T., & Kakigi, R. (2005). Changes in the centrifugal gating effect on somatosensory evoked potentials depending on the level of contractile force. Experimental Brain Research, 166(1), 118–125.

Wersinger, E., & Fuchs, P. A. (2011). Modulation of hair cell efferents. Hearing Research, 279(1–2), 1–12.

Williams, S. R., Shenasa, J., & Chapman, C. E. (1998). Time Course and Magnitude of Movement-Related Gating of Tactile Detection in Humans. I. Importance of Stimulus Location. Journal of Neurophysiology, 79(2), 947–963.

Chapter 4 | Conclusions

Over the course of my dissertation project, I have investigated the process of elaboration of sensory representations occurring at the first synapse level along the dorsal-column medial lemniscus pathway, namely the cuneate nucleus. These studies constitute the first characterization of the tactile response properties in the CN of primates. In addition, we were among the first to successfully investigate brain stem nuclei at the single-neuron level in active behaving macaques. The approach we developed allowed us to address questions which had been experimentally inaccessible and thus potentially accelerate future studies in this field. The following are among the most significant: first, we found that individual CN neurons receive convergent input from multiple afferent classes such that the submodality convergence observed in cortex is at least in part inherited from its inputs. Second, we observed that CN exhibit inhibitory responses, which is not observed at the periphery. In addition, the existence of inhibitory inputs to CN is demonstrating that processing is occurring at this stage. Thirdly, we found that the population-level sensory representations in CN constitute an intermediary between their peripheral and cortical counterparts, and are more similar to cortical ones. Lastly, cutaneous responses to tactile stimulation that are not directly relevant task goal are inhibited while task-goal related tactile inputs are elevated during movements at the level of brain stem nuclei. Such a bidirectional modulation mechanism would help with the fluent execution of behavior by improving discrimination. Together, these findings revolutionized our understanding of how tactile representations are transformed as they ascend the somatosensory pathway by demonstrating that the CN is not a simple relay station for tactile signals but rather plays an active role in processing, which is inherently against all textbooks's view of CN as a passive relay station. We anticipate that the gained knowledge of the underlying topography and response properties of CN will spur an entire program of research, including but not limited to the development of bionic touch via subcortical nuclei stimulation (Bologna et al., 2011; Richardson et al., 2016).

4.0.1 References

Bologna, L. L., Pinoteau, J., Brasselet, R., Maggiali, M., & Arleo, A. (2011). Encoding/decoding of first and second order tactile afferents in a neurorobotic application. Journal of Physiology-Paris, 105(1-3), 25-35.

Richardson, A. G., Weigand, P. K., Sritharan, S. Y., & Lucas, T. H. (2016). A chronic neural interface to the macaque dorsal column nuclei. Journal of neurophysiology, 115(5), 2255-2264.